A Study of the Uptake of Cu^{2+} by Calcium Silicate by Batch and Continuous Reactors for Potential Commercialisation

By

Giancarlo Mario Barassi Infante

VICTORIA UNIVERSITY OF WELLINGTON
Te Whare Wānanga o te Ūpoko o te Ika a Māui

A thesis

submitted to the Victoria University of Wellington

in fulfilment of the requirements for the degree of

Doctor of Philosophy

Victoria University of Wellington

2013

Chapter 4 , Mining Waste Characterisation, Simulation and Treatment with NCaSil

4.1 Mining waste

During mining operations large amounts of solid, liquid and even gaseous waste effluents are produced. It is estimated that every 1 tons of metallic copper produced, generates 350 tons of sterile rocks, 140 tons of low copper content rock, 66 tons of solid residues and 57 tons of lixiviation residues [87]. The process by which copper is produced varies depending on the type of mineral that is being extracted. Appendix A-4 to A-7 show flow sheets for the production of copper from different types of minerals.

Generally, copper production involves several steps aimed at releasing the copper containing mineral (usually copper sulfides) from the mined ore. Often grinding is the first step and subsequent steps involve the use of chemicals to release the element of choice. The flow sheets presented in appendix A-4 to A-7 show that multiple stages during the production of copper release liquid wastes (enclosed in red boxes), each of these have in common a low pH due to the presence of sulfuric acid in some of the stages of production. Arsenic is also very common in mining tailings since most copper sulfides are associated with arsenic bearing rocks [88].

New Zealand and Chile both have mining histories. While New Zealand moved from mining into agricultural production, Chile has given great importance of the exploitation of minerals providing the country with large revenues. Chile is the world's largest producer of copper which is mainly extracted in large scale mines but also in several other small and medium scale mines [89]. Large scale mines usually try to comply to

international environmental management systems. Most companies have an ISO 14001 accreditation, to demonstrate that they take their responsibilities seriously [90]. In contrast small and medium scale mines do not follow international accreditation as it represents a huge investment of resources and is not compulsory, which could lead to a loose management of waste disposal.

Moreover, mining activity in New Zealand in the last century resulted in high metal ion content in river basins [91]. Often in the past after a mine was closed, no rehabilitation was carried out, leaving minerals exposed to oxidation and further leaching of metal ions into bodies of water. Wilson *et al*. [92] have reported that a historic antimony mine in Marlborough, New Zealand, contributed to an arsenic concentration three times larger in the leachate than in the groundwater entering the mine. Weber *et al*. [93] described that nickel was associated with acid rock drainage in coal mining activities in the West Coast of New Zealand. Gold mining in Reefton, New Zealand, has led to the leaching of arsenic out of rocks from the mining waste, although natural attenuation of the concentration downstream has been reported [94].

Traditional mining in the northern regions of Chile has led to the contamination of marine environments due to mining tailing discharges. Ramirez *et al*. [95] have reported the presence of metal ions in marine sediments on the coast near El Salvador, Chile, in the range of 7.2-985 mg kg^{-1} of Cu and 746-22739 mg kg^{-1} of Mn, respectively, which have been attributed to mining tailings. Some bays, such as la Herradura and Tongoy, have been reported to contain high concentrations of copper and iron ions [96]. The presence of the latter ion at Tongoy Bay was due to iron dust from the iron mineral loading wharf located in the bay, while the presence of copper ions could be associated to the fact that Tongoy was a copper port in the past.

4.1.1 Acid mine drainage

Acid Mine Drainage (AMD), also called Acid Rock Drainage (ARD), is a naturally-occurring effluent produced when sulfide-bearing minerals are exposed to oxygen and water [46]. The generation of AMD is associated with iron sulfide containing rocks. This process can be enhanced by mining exposing more rock to air or by the presence of naturally occurring bacteria (e.g. *thiobacillus ferrooxidans)* [97] which accelerate the breakdown of sulfide ores. This is a common process in old abandoned mines where no terrain rehabilitation programme has been undertaken. It is difficult to estimate the potential for a mine to generate AMD effluents, but in most of the cases AMD is related to the following key factors present in sulfide ores: water or high humidity and oxidant

availability (e.g oxygen). Presented below is the general mechanism by which AMD is generated from pyrite ore [46, 98].

Oxidation of the sulfide mineral in the presence of water,

$$FeS_2 + 3.5O_2 + H_2O \rightarrow Fe^{2+} + 2SO_4{}^{2-} + 2H^+ \quad \text{(eq. 4.1)}$$

Further oxidation from ferrous to ferric ion occurs if the surrounding environment is sufficiently oxidizing,

$$2Fe^{2+} + 0.5O_2 + 2H^+ \rightarrow 2Fe^{3+} + H_2O \quad \text{(eq. 4.2)}$$

At pH values between 2.3 and 3.5, ferric ions precipitate as $Fe(OH)_3$ and jarosite $KFe_3(SO_4)_2(OH)_6$, leaving little Fe^{3+} in solution while simultaneously lowering the pH,

$$Fe^{3+} + 3H_2O \rightarrow Fe(OH)_{3\ solid} + 3H^+ \quad \text{(eq. 4.3)}$$

The remaining Fe^{3+} may oxidize additional pyrite,

$$FeS_2 + 14Fe^{3+} + 8H_2O \rightarrow 15Fe^{2+} + 2SO_4{}^{2-} + 16H^+ \quad \text{(eq. 4.4)}$$

The presence of sulfur degrading bacteria will catalyse the reaction by lowering the pH through the production of H_2SO_4 and preventing ferric hydroxide precipitation. Since the reaction involves the release of iron ions and other metal ions most AMD affected sites are often yellow to red in colour. In many cases the severity of AMD is related to the pH and is considered moderate in the range of pH 2-4. Generally the characteristics of AMD change from site-to-site, but low pH, high concentrations of iron ion as well as aluminium and manganese ions are often found. However, the concentration of heavy metal ions may vary depending on the minerals present at each site since solubility of metal ions is enhanced by low pH and oxidizing environments.

4.1.2 Technologies to address mining waste waters

There are several treatments for mining waste waters, but since all residual effluents are characterized by low pH values and a high metal ion content, most treatments include a basification stage raising the pH to a value near 9.5 [99]. The most common basification process involves the addition of lime and the use of settling ponds. An example of such a method is shown in appendix A-8. This method is low cost if enough space is available, but it has drawbacks since bad aeration leads to an incomplete removal of ferrous ions. This system also lacks flow control and is susceptible to wind which could possibly lead to a non-compliant discharge. Moreover, it is vulnerable to floods due to

rainfall. A pumping station or gate system may be added but this increases the overall cost. Hence this is not the most desirable system.

When the ore is roasted in the furnace a gas stream is generated containing mainly SO_2 and suspended solid particles rich in copper, arsenic and other metal ions. This gas stream is used to make concentrated sulfuric acid but it has to be cleaned in a prior step with water scrubbers and passed through an electrostatic precipitator in order to prevent the contamination of the catalyst used further in the process. A liquid effluent is generated at this stage which is commonly known as acid plant 'blow-down' or also referred to as weak acid in the literature [100-102]. This effluent usually has pH values < 1 and high contents of arsenic, sulfate (1 - 10 g L^{-1}) and transition metal-ions [101]. The term might have arises due to the generation of commercial sulfuric acid downstream of the process. The method to treat this "blow-down" effluent is shown in A-9 and is based on a precipitation step accompanied by the addition of a flocculant, facilitating the separation. This design helps to readily precipitate arsenic as $Ca_3(AsO_3)_2$ and $Fe(AsO_3)$. This offers an improvement over the pond method as it allows more control over the final characteristic of the resultant discharge effluent.

BAMAG GmbH has designed a variant of the former process making it possible to produce clean gypsum by utilizing the weak acid [101]. This helps to decrease the costs by generating a by-product and reducing the volume of the solid waste. A schematic of such a process is given in appendix A-10. Here the pH value is set to 1 with lime allowing the formation of $CaSO_4$ and at the same time avoiding the precipitation of arsenic and transition metals. Once the product is formed, it is recovered by filtration and dewatered, being ready to be sold. The remaining effluent is treated under the standard scheme previously mentioned. This new method reports good results for weak acids containing a large amount of sulfates and low content of arsenic ions < 1 g L^{-1}. The process has been implemented at Atlantic Copper, Huelva, Spain reducing the cost of waste disposal as expected.

Another chemical method available to remove metal ions is based on the precipitation of metal ions as sulfides by adding NaS_2, NaHS or H_2S. In the literature the latest process regarding this method involves the biogeneration of H_2S [103]. Here, the production of hydrogen sulfide is achieved from sulfate or sulfur through a bacterium catalyzed redox reaction. Usually acetic acid is used as the electron donor in the presence of *desulfuromonas acetoxidans* bacteria which grow using the energy released by linking the oxidation of acetate to the reduction of elemental sulfur. Eq. 4.5 and 4.6

show the simplified equation for underlying reactions of sulfates and sulfur with acetic acid.

$$SO_4^{2-} + CH_3COOH + 2H^+ \rightarrow HS^- + 2HCO_3^- + 3H^+ \quad \text{(eq. 4.5)}$$

$$4S^0 + CH_3COOH + 2H_2O \rightarrow 4H_2S + 2CO_2 \quad \text{(eq. 4.6)}$$

In appendix A-11 is shown a schematic of the process. The precipitation of metal ions as sulfides is often claimed to be superior compared to the ones involving the addition of lime in terms of sludge volume, reusability of the sludge and effluent quality. The advantages can be summarized as:

- High reactivity of sulfides with heavy metal ions and very low solubility of the metal sulfides over a broad pH range resulting in lower effluent concentrations.
- Sulfide precipitation, unlike hydroxide precipitation, is relatively insensitive to the presence of complexes and most chelating agents.
- The method can remove chromates and dichromates without preliminary reduction of the chromium to the trivalent state.
- A high degree of selective metal precipitation is achievable with sulfide, by controlling the pH.

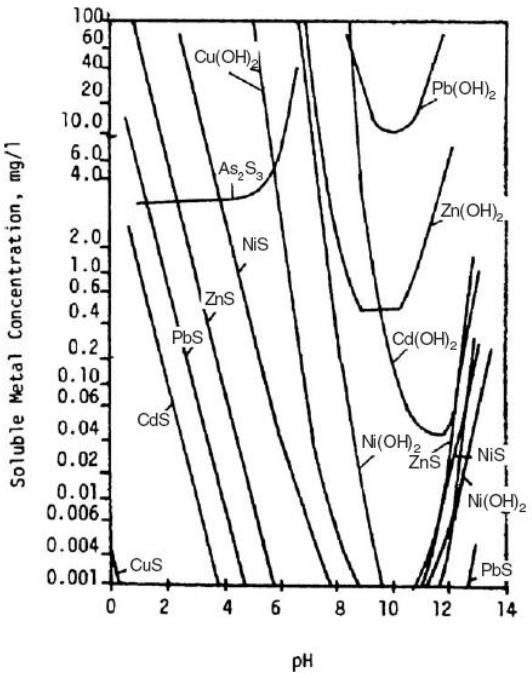

Figure 4.1: Comparison between metal hydroxides and metal sulfides equilibrium concentration taken from reference [103].

In Figure 4.1 is shown a speciation diagram comparing the equilibrium concentrations of metal hydroxides and metal sulfides. The solubility of metal sulfides is not only

much lower but also it is effective over a wider range of pH, thus having better control over the precipitation and generating a cleaner discharge effluent.

Metal sulfide sludges generally are easier to dewater and facilitate further processing due to a formation of a thicker sludge than metal hydroxides. This design, as discussed above, can selectively precipitate CuS and NiS separately by controlling the pH generating a reusable or sellable sludge. Drawbacks from this process come from the use of toxic reagents such as H_2S which involves the use of more complex equipment to avoid leakages.

It is possible to say that recent technologies aim to not only remove metal ions from the solution but also to generate a by-product that can be sold and help to reduce the cost involved in waste treatment and disposal. Hence, this chapter focuses on the recovery of Cu^{2+} ions from mining waste waters. Taking into consideration results obtained in Chapter 3, where high concentration of Cu^{2+} (higher than 3.9 mmol L^{-1}) generated copper sulfate hydroxide species, the above mentioned weak acid presents an interesting waste to be studied and treated due to high concentrations of Cu^{2+}.

4.1.3 Weak acid production at *El Teniente* mine, Chile

El Teniente is a copper mine operated by the state owned company *Corporación Nacional del Cobre* (CODELCO) located in the Andes mountains range near Rancagua in Chile. The mine extracts copper and molybdenum sulfides, which are separated by ore selective flotation. El Teniente is considered to be the world's largest underground copper mine in size and 5th in terms of production of copper [100]. It operates two 'Teniente-type' furnaces, which are 22 meters long and 5 meters wide, located at Caletones 34º 07' S and 70º 27' W near the mining site, granting the mine a production capacity of 400,000 tons of copper per year [100].

Roasting of sulfide containing minerals generates gases with a high content of SO_2 and suspended particulate material. The chemical composition and physical characteristics of this gaseous effluent are in direct relation to the mineral being roasted and the furnace employed. In the past, no post-treatment of the gases released from the furnaces was carried out, which led to the release of gases containing SO_X and particulate material containing arsenic and heavy metals to the surrounding environments. The contribution to pollution derived from copper roasting in this particular region of Chile was investigated by Romo-Kröger et al. [104], who reached the conclusion that aerosols containing Cu, Zn, As and S were produced by the smelter, contributing significantly to the atmospheric contamination in the area. Another study showed that these aerosols

were transported away from the site by wind currents and contributed to abnormal concentrations of heavy metal and metalloids in surrounding rivers and waterways [105].

In order to meet current environmental standards in Chile [90, 106] for the discharge of gases the exhaust from the smelter is thoroughly cleaned and sulfur is transformed into a valuable commodity before the remainder of the gases is released into the environment. Most sulfide smelters have a sulfuric acid plant attached to make use of the generated SO_2 to produce sulfuric acid as a by-product. Commonly, sulfuric acid plants also help to recover heat from the exhaust current. In the case of El Teniente the gas is only cooled down and cleaned using a water mist without any attempt at recovering thermal energy being undertaken. During the gas-cleaning step, the exhaust gas is channelled through water scrubbing towers operating in counter current. As the gases cool down, particulate material and some of the SO_2 including other gases are trapped in the condensate of the water vapour generating the weak acid. The next step of the exhaust purification involves an electrostatic precipitator, which further removes any fine particles suspended in the gas stream. This is important as the SO_2 current must be free of any particulates before contacting it with a V_2O_5 catalyst which oxidizes SO_2 to SO_3, as particles could damage the catalyst or impede gas flow. Finally, the freshly generated SO_3 is contacted with water to form concentrated sulfuric acid.

The copper sulfides targeted for copper mining at El Teniente are associated with arsenic containing ore. Hence, the weak acid from El Teniente is expected to contain high concentrations of arsenic and sulfate. The weak acid stream is regularly analysed for these species and for its acidity. The weak acid is treated in order to meet environmental discharge requirements described by *Decreto Supremo 90* in Chile [14]. The chemical treatment of the weak acid consists of two stages. The first one involves the addition of milk of lime $Ca(OH)_2$ to precipitate heavy metals as hydroxides $M^{n+}(OH^-)_n$, sulfate as gypsum $CaSO_4$ and arsenic as calcium arsenite $CaAsO_3$. The second stage involves the addition of ferric chloride and hydrochloric acid to precipitate any remaining arsenic from solution. The resulting precipitates form a sludge, which will be referred to in this work as ‘dirty gypsum’ and contains a mixture of calcium sulfate, calcium arsenite and ferric arsenite [102]. These inorganic salts have low solubility products. Therefore, they can be ‘safely’ disposed of on landfills with only minor leaching issues occurring.

Although weak acid is periodically surveyed at El Teniente to determine the content of SO_4^{2-}, As and suspended solids, little attention has been given to the presence of metals

in both liquids (ions) and suspended solids (microparticles, nanoparticles) in the waste. This particulate material containing heavy metals could pose a threat to the environment. Even after being occluded by the dirty gypsum during the addition of milk of lime to the weak acid, these particles could be transported away by several mechanisms similar to those proposed by Romo-Kröger in his study [105].

In the literature most studies of the gaseous effluent have placed emphasis on the recovery of valuable metal ions from the flue dusts collected downstream at the electrostatic precipitator [107-109] and have neglected the weak acid waste. This work focuses on the acid plant 'blow-down', also known as weak acid, generated by water scrubbing towers. The characterisation of this waste will help to establish if it poses a hazard for the environment, and potential for metal recovery or treatment.

4.1.4 Operation of cooling towers

Weak acid samples were collected from the two cooling towers at El Teniente's sulfuric acid plant. Both towers produce an overall of 500 m^3 day^{-1} of weak acid with an average temperature at the outlet of 328 K. Similar flows have been reported for other plants, for example, Toyo's smelter in Japan generates 300 m^3 of weak acid per day [110].

The liquid was light blue in colour containing particulate material in suspension, which settled within minutes after sample collection. Although the liquid portion of the sample was light blue colour (characteristic of copper sulfate in solution), little attention has been paid to the metal content of this effluent in the past. A potential reason for this neglect is that the light blue colour becomes easily masked by the suspended solid particles, which lend fresh samples a grayish to light orange coloration. The other reason might be that the dissolved copper concentration of the effluent was estimated to be quite low, which makes this waste unattractive for hydrometallurgical processes and copper recovery.

CODELCO staff members provided operational data for the two water scrubber towers at the acid generation plant in El Teniente mine, collecting data daily over a period of 6 months. Appendix A-12 to A-17 show Stewart charts, also known as control charts for Plant 1 recording the total concentrations of arsenic, sulfate and weight percentages of suspended solids from May 2010 until October 2010.

Table 4.1 presents the statistical parameters of the operation and summarizes the values presented in appendix A-12 to A-17. Values of ±2σ, lower and upper warning limits (LWL and UWL), and ±3σ, lower and upper action limits (LAL and UAL), for some of the parameters are not shown since they gave negative values and there cannot be negative concentrations.

Table 4.1: Summary of the presented control chart parameters for the weak acid generated at Plants 1 and 2 at El Teniente.

	Plant 1			Plant 2		
	total As [g L^{-1}]	**SO_4^{-2} [g L^{-1}]**	**suspended solid content [%wt]**	**total As [g L^{-1}]**	**SO_4^{-2} [g L^{-1}]**	**suspended solid content [%wt]**
Average	6.1	43.2	0.23	6.5	68.7	0.97
Std. dev.	2.9	10.0	0.63	1.2	11.6	0.95
min	1.8	11.1	0.03	3.1	39.8	0.06
max	65.0	73.8	13.00	11.5	108.5	9.82
UWL	11.9	63.1	1.49	9.0	91.9	2.88
LWL	0.3	23.2	-	4.0	45.5	-
UAL	14.7	73.1	2.12	10.3	103.5	3.83
LAL	-	13.2	-	2.8	33.9	-

From Appendix A-12 to A-17 it can be seen that on the date when the samples studied throughout this article were collected, the plant was operating within 1σ of the average, indicating that the samples collected present an insight into a normal operational day.

Plant 1 shows less data dispersion than Plant 2 for the total As and SO_4^{2-} concentrations. On the 16th of July, 2010, Plant 1 reported the maximum value for As during the monitored time with a concentration 65 g L^{-1} for this species in solution, as shown in

Table 4.1. This value contributed to the large standard deviation of 2.9 g L^{-1} of arsenic for this plant. The average amount of suspended solids in Plant 2 is four times larger than in Plant 1. Furthermore, the concentration of SO_4^{2-} reached a peak value of 108.5 g L^{-1} on the 11th of August 2010 (not shown in the graph). Despite these differences, overall, both plants operated steadily. There were 10 events where the parameters exceeded LAL or UAL values (located at ±3σ from the average) during the monitored period.

A study by Inami et al. [111] on the weak acid generated at the Toyo smelter, Japan, reported the following values for the major constituents: 80 – 150 g L^{-1} H_2SO_4, 0.5 - 1 g L^{-1} Cu, 2 – 5 g L^{-1} As, 0.5 – 2 g L^{-1} Zn and 1 – 5 g L^{-1} Cl. The concentration of arsenic and sulfate present in the supernatant of El Teniente's weak acid is higher compared to those reported for the one generated at Huelva, Spain and Toyo, Japan [101]. In the case of arsenic concentrations, the Chilean weak acid contains on average seven times the amount of arsenic compared to the concentrations used by BAMAG GmbH to emulate the Spanish weak acid [101]. El Teniente's average total As concentrations are 20 to 325% larger than those present in the weak acid from the Toyo's smelter. Furthermore, the SO_4^{2-} concentration observed in the weak acid waste from El Teniente is approximately half of that present in the Toyo's smelter weak acid. These differences could be attributed to the quality of the ore being processed at the smelters, implying that Chilean ore has potentially a lower grade than the ore being roasted at the above mentioned Spanish and Japanese smelters.

4.1.5 Chemical characterisation of the liquid phase, the supernatant

A representative sample of weak acid waste was collected by CODELCO at the sulfuric acid plant at El Teniente. The sample was filtered and the liquid phase was analyzed in a private laboratory in Chile. The results from the chemical analysis of the liquid phase of the sample are displayed in Table 4.2.

Table 4.2: Chemical analysis of the liquid portion of the sample.

Analyte	unit	value
Al^{3+}		113
As, total*		6.0
Ca^{2+}		1449
Co, total		0.103
Cr, total		0.076
Cu^{2+}		562
Fe, total		185
K^{+}		467
Mg^{2+}	mg L^{-1}	39.7
Mo, total		50.3
Na^{+}		152
Ni^{2+}		0.402
Pb, total		22
V, total		<0.008
Cl^{-}		475
NO_3^{-}		<0.20
SO_4^{2-}		32800
Acidity	mg L^{-1} $CaCO_3$	2970
COD	mg L^{-1}	3023
Conductivity	µS cm^{-1}	334000
pH		0.45

*value taken from Codelco report due to low concentration in

Table 4.2 shows that the major components, with concentrations >100 mg L^{-1}, in the weak acid are H^{+}, Cu^{2+}, SO_4^{2-}, Ca^{2+}, total Fe, total As, K^{+}, and Al^{3+}. Consequently, this liquid waste can be categorized as extremely acidic and high in metal content according to the Flicklin diagram [112]. The low pH value of 0.45 may be explained from the formation of sulfurous acid and sulfuric acid due to the presence of SO_2 in solution. The reactions of SO_2 in presence of water in anoxic and oxidizing conditions are represented in eq. 4.7 and eq. 4.8 respectively,

$$SO_{2\,(g)} + H_2O \rightarrow H_2SO_3 \qquad \text{(eq. 4.7)}$$

$$SO_{2\,(g)} + \tfrac{1}{2}\, O_{2\,(g)} + H_2O \rightarrow H_2SO_4 \qquad \text{(eq. 4.8)}$$

Taking into consideration that both of these acids are polyprotic in nature, the degree of protonation of the acid in solution will depend on their pK_a. Sulfurous acid has a pK_a value for the first deprotonation of 1.90 and for the second deprotonation of 7.29. Therefore it is most likely that the species found in solution will be H_2SO_3. On the other hand, sulfuric acid has a pK_a value for the first and second deprotonation of -3.0 and 1.99 respectively, so it is most likely that the predominant species present in solution will be HSO_4^-. For this study it was assumed that a mixture of H_2SO_3 and HSO_4^- was present in the sample.

The high value for the Chemical Oxygen Demand (COD) of 3023 mg L^{-1} may be attributed to the presence of As^{3+} that can be oxidized to As^{5+}. Also, SO_3^{2-} may contribute to the COD considering that it can be oxidized to SO_4^{2-}.

Taking into consideration the volume of weak acid produced per day and the concentration reported in Table 4.2, it can be calculated that approximately 100 tons of copper are expelled through the fumes of this copper smelter into the weak acid waste per year. Considering the actual copper price (6.5 USD kg^{-1}) this presents a significant loss of the metals and economical value. At Toyo's smelter, copper ions present in the weak acid are recovered as copper sulfide by the addition of NaHS [110].

4.1.6 Characterisation of the solid phase: suspended particles.

Results from the chemical analysis of the digested sample using FAAS and ICP-OES are shown in Table 4.3.

Table 4.3: Concentration of different metals and metalloids found in the suspended solids of the weak acid waste collected at El Teniente.

Analyte	Concentration [mg g^{-1}]
Al	0.2480 ± 0.0006
As	4.765 ± 0.019
Ba	<LOD
Bi	3.493 ± 0.010
Ca	2.492 ± 0.052
Co	0.08 ± 0.078
Cr	<LOD
Cu	10.04 ± 0.34
Fe	6.48 ± 0.29
Hg	0.2170 ± 0.0007
K	32.20 ± 0.15
Mg	0.04900 ± 0.0003
Mn	0.048 ± 0.0387
Mo	<LOD
Na	0.722 ± 0.008
Nb	0.736 ± 0.712
Pb	635 ± 17
Re	<LOD
Sb	0.868 ± 0.004
Sn	0.1100 ± 0.0006
Ti	0.179 ± 0.014
V	0.416 ± 0.004
Y	<LOD
Zn	0.643 ± 0.104
Zr	0.608 ± 0.003

Cu, Fe, and Pb were measured using FAAS, all other analytes were measured in ICP-OES.

The highest concentration is that of lead with a concentration of 635 ± 17 mg g^{-1}. Followed by a fair amount of potassium, copper and iron in the sample with concentrations of 32.20 ± 0.15, 10.04 ± 0.34 and 6.48 ± 0.29 mg g^{-1} for each metal respectively. Arsenic and bismuth were present in concentrations of 4.765 ± 0.019 and 3.493 ± 0.010 mg g^{-1}, respectively. On the other hand, barium, chromium, molybdenum, rhenium, silicon and yttrium were below the limit of detection (LOD) of the analysis methods employed. The proportions of all other analytes were between the LOD and 1 mg g^{-1}.

High concentrations of lead might be explained considering that the ore molybdenite (MoS_2) often occurs in combination with small amounts of wulfenite ($PbMoO_4$). This is consistent with molybdenum being present in the liquid phase of the sample as shown in Table 4.2. Also galena, a lead sulfide (PbS), should be considered as a possible source. It is likely that when molybdenum sulfide is separated from copper sulfides by selective ore flotation, wulfenite stays with the copper sulfides as wulfenite and/or galena are less hydrophobic (different wettability) than the molybdenite. As a result, lead will be released when copper ore is roasted in the smelter. This is supported by the concentration of molybdenum in solution (50 mg L^{-1}).

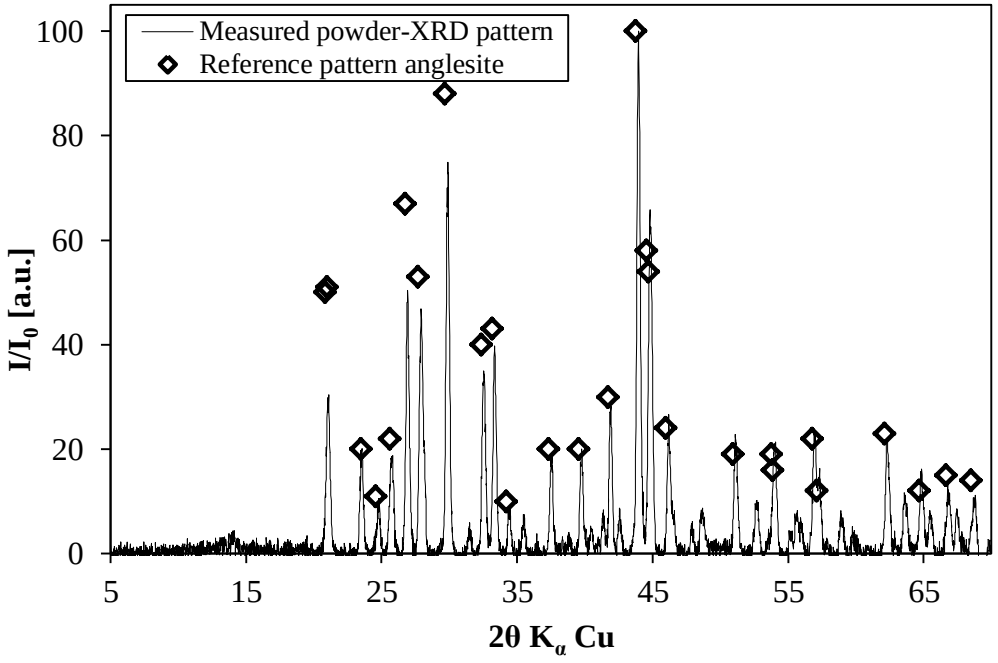

Figure 4.2: XRD pattern for the suspended solids from the weak acid sample. Refer to section 2.4.1 for sample collection.

A small dried sample of the suspended solids of the weak acid was analysed using powder-XRD. Figure 4.2 shows the retrieved pattern. The reflections fitted those of anglesite ($PbSO_4$) (PDF FILE 00-036-1461) scoring 85% in the search and match option of the PANALYTICAL data processing software. This is in accordance with other findings where the anglesite is reported to form in the exhaust during the smelting of ore containing lead [113]. Some of the remaining reflections fitted compounds such as arsenic trioxide and iron sulfite. However, the score for the fit of these structures was very low even after subtraction of the anglesite pattern. Some of the standard patterns on record were of too low quality to unambiguously identity specific structures. Specifically, reflections associated with arsenic trioxide were discarded, as the structure of this compound is polymorphous.

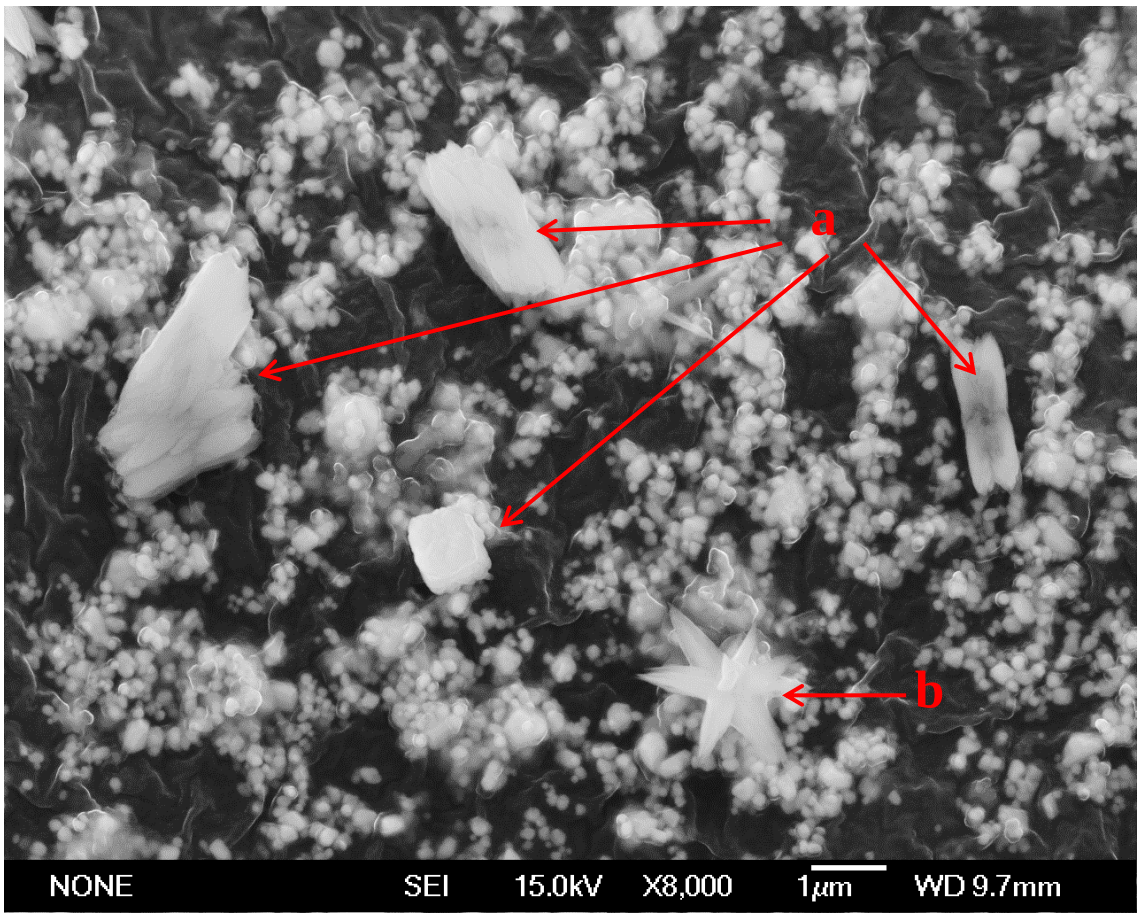

Figure 4.3: Three different types of structures observed in the suspended solids: a) rectangular rhomboids; b) star shapes; and unlabeled sub-micron particles (bright, white dots and clusters of dots). Refer to section 2.4.1 for sample colletion

Scanning electron microscopy (SEM) analysis revealed three types of solid structures. The largest structure observed was a rhomboid as shown in four spots (marked as a) in Figure 4.3) in the backscattered image of the dried suspended solids sample. This structure was composed mainly of sodium, sulfur and oxygen as shown by energy dispersive spectroscopy (EDS) and associated X-ray maps (Figure 4.4). The high correlation of the three elements represented as white in the convoluted representation indicated that this structure probably is crystalline sodium sulfate. There was no evidence for crystals of sodium sulfate in the XRD pattern of the suspended solids. Considering the solubility of sodium sulfate, it was thought that these crystals formed during the drying step of sample preparation from the liquid films covering the suspended solids, as said solids were not washed.

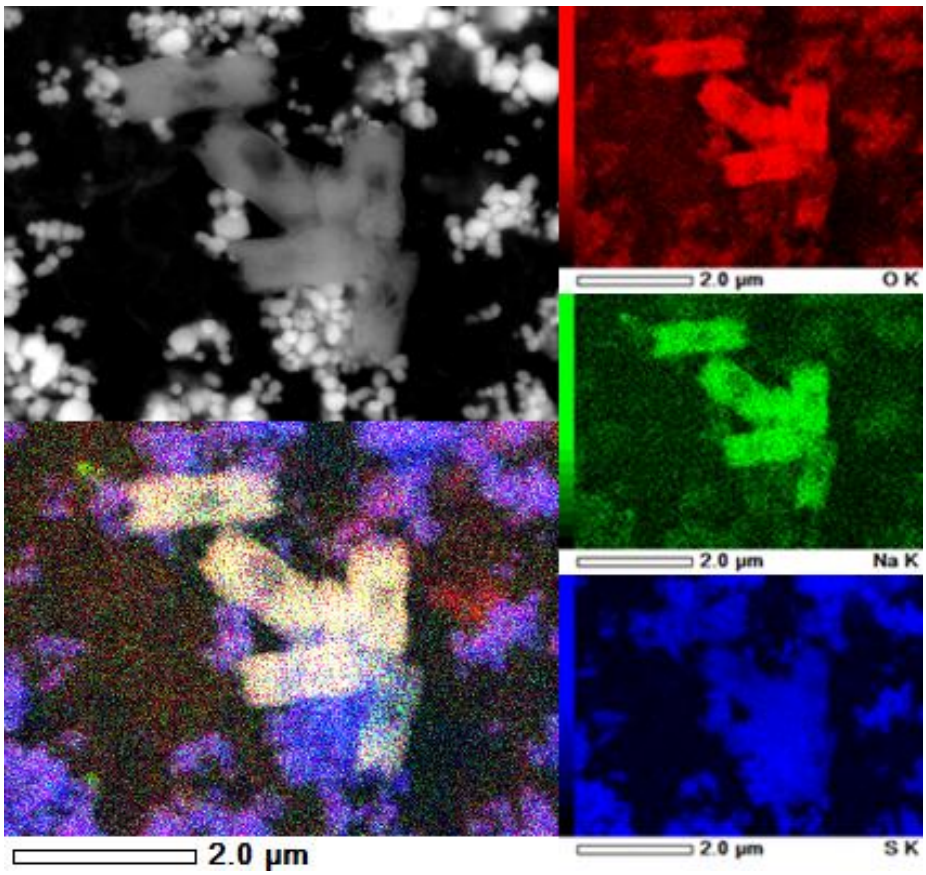

Figure 4.4: SEM-EDS imaging of the rhomboid type of structures found in the suspended solids. Presence of sulfur is shown in blue, oxygen in red and sodium in green. The overlay of oxygen and sulfur is represented as purple and the overlay of oxygen, sulfur and sodium as white. A backscattered electron image is presented in grayscale in the top left corner for orientation.

The second type of structure corresponded to a star shaped particle as shown in the spots marked as b) in Figure 4.3. It had a high content of arsenic, calcium and oxygen as evidenced by EDS. An X-ray overlay map produced using the EDS data showing the structure in white colour in the convoluted representation in Figure 4.5, suggesting it to be a calcium arsenate crystal. This could not be corroborated by XRD as the pattern did not match calcium arsenate peaks. The star-shaped particles were unstable and suffered irreversible damage during electron microscopy, which suggests that the particle might have lost the water molecules bound in their lattice. It is likely that calcium arsenate was present in the suspended solids in amorphous form and only crystallized and decomposed during sample preparation and analysis.

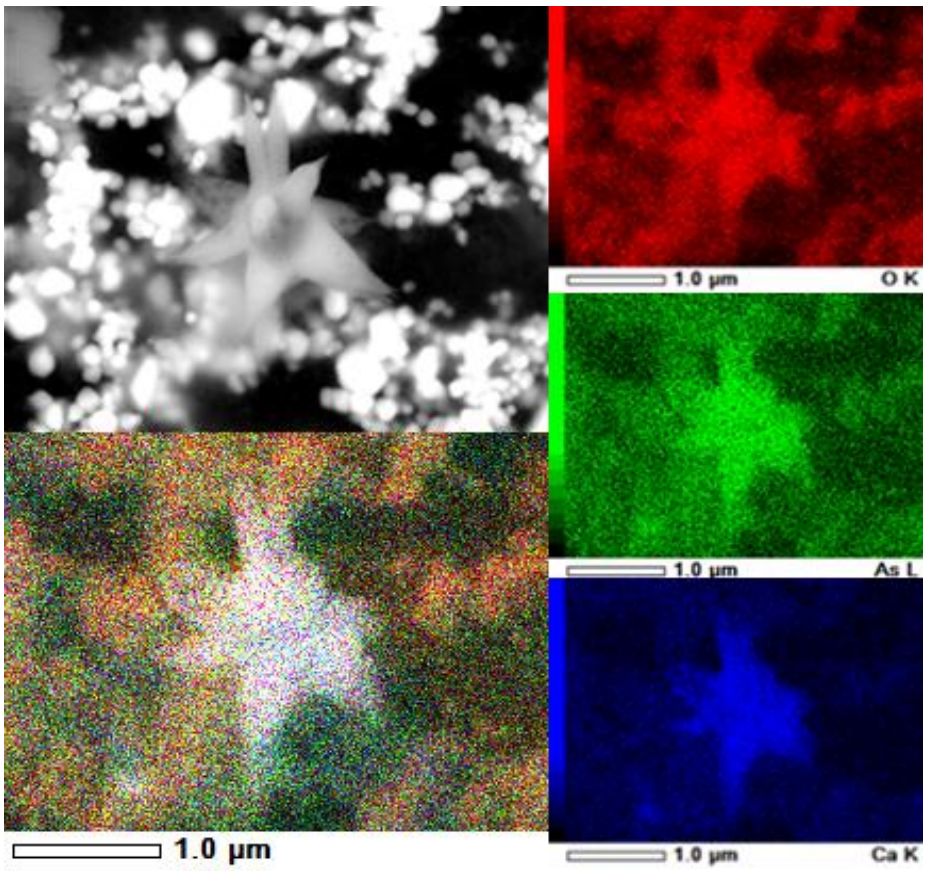

Figure 4.5: SEM-EDS imaging of the star shaped type of structures observed in the suspended solids. Presence of calcium is represented in blue, oxygen in red and arsenic in green. The overlay of these three elements is shown in white. A backscattered electron image is presented in grayscale in the top left corner for orientation.

The third type of particles represents the predominant species found in the suspended solids. These particles are sized in the range from 50-500 nm. These sub-micron particles are noticeable in Figure 4.3 as bright, white dots and clusters of dots. Considering that commonly used microfiltration membranes in chemical analysis have a cut-off point of 0.45 µm, it is most likely that these particles bypassed any filtration and gas purification steps carried out in the sulfuric acid plant. It is also likely that some of these sub-micron particles will have remained in the filtrate and, hence, contributed to the quantification of sulfate in solution during the analysis presented earlier. The images of the sub-micron particles present them in a strong contrast to the background, especially when the backscattered electron detector of the SEM is employed (Figure 4.3). This suggests that the constituents are elements of high atomic mass. Figure 4.3 shows the difference in the contrast between the background and the flower type crystals, the rhomboid crystals and the sub-micron particles. Furthermore, EDS analysis in Figure 4.6 suggests that the sub-micron particles are mainly composed of lead, sulfur and oxygen. XRD results shown in Figure 4.2 confirm this, indicating that the main component of the suspended solids of the weak acid is anglesite ($PbSO_4$). Moreover, the

third type of particles did not suffer structural changes during any of the analysis methods suggesting they were formed under high temperature conditions.

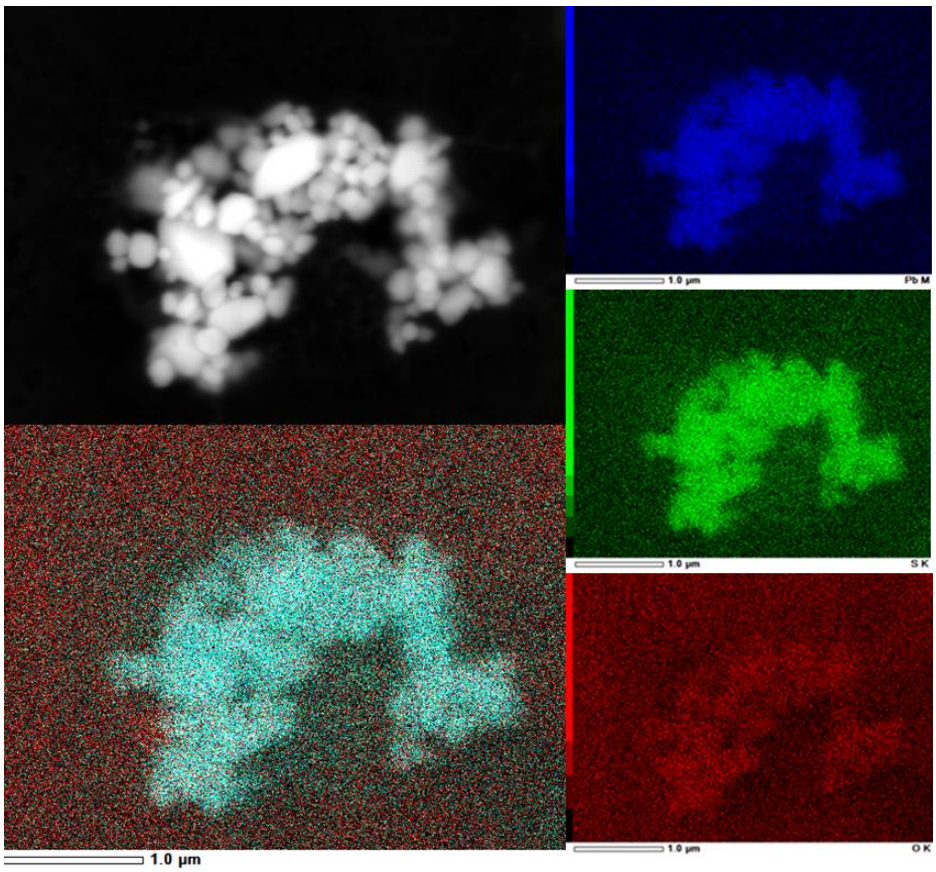

Figure 4.6: SEM-EDS imaging of the sub-micron particles. Lead is represented as blue, oxygen as red and sulfur as green. The overlay of oxygen, sulfur and lead mapping is represented in light blue. A backscattered electron image is presented in grayscale in the top left corner for orientation.

The findings of this study differ from those obtained by Roca et al. [107] reporting on the flue dust coming from flash smelting furnace. The collected particles were of a complex structure containing multiple mainly copper based minerals such as cuprospinel ($(Cu,Mg)Fe_2O_4$), chalcocyanite ($CuSO_4$), delafossite ($CuFeO_2$), zincosite ($ZnSO_4$), claudetite (As_2O_3), arsenolite (As_2O_3) and tenorite (CuO). Furthermore, some particles found in the flue dust were up to two orders of magnitude larger than the ones present in El Teniente's weak acid presented here. Roca et al found that the particles contained a high concentration of copper that could be easily leached out with water. In contrast to their findings, the chemical analysis revealed that the solid phase of the sample collected at El Teniente contained, as was shown in Table 4.3, a considerably smaller quantity of copper. Taking into consideration the concentration of copper in the solid phase (10.04 ± 0.34 mg L^{-1}) and comparing it to the liquid phase (562 mg L^{-1}) of El Teniente's weak acid, one might assume that copper ions present in solution leached out from particles, when they were surrounded by water inside the cooling tower.

From an environmental and toxicological point of view, the solid phase represents a serious hazard, not only due to its high concentration in lead but also due to the fact that it is composed of sub-micron particles. It is most likely that upon treatment of the weak acid these sub-micron particles are occluded in the 'dirty gypsum'. The immobilization of the sub-micron particles inside the gypsum has to be established. In the case that it is easy to dislodge them from the gypsum, sub-micron particles could easily be transported away from the dirty gypsum landfill to pose a health or environmental threat due to their particle size.

In a different aspect, CODELCO reported difficulty in the first stage of the weak acid treatment, presenting slow kinetics in the precipitation of SO_4^{2-} as calcium sulfate. Usually, an excess of milk of lime had to be used in order to precipitate this anion. This could be due to sulfate being present to a large extent as colloidal sub-micron particles. This means that instead of precipitating SO_4^{2-} ions from solution (homogeneous reaction), represented in eq. 4.9, calcium would also have to react with the surface of the sub-micron particles (heterogeneous reaction) as represented in eq. 4.10. The consequence is that the formation and precipitation of gypsum is considerably slower than expected and results in a poorer product containing sub-micron particles of lead sulfate and lead impurities.

$$Ca^{2+} + SO_4^{2-} \rightleftharpoons CaSO_{4(s)} \qquad \text{(eq. 4.9)}$$

$$Ca^{2+} + PbSO_{4(s)} \rightleftharpoons CaSO_{4(s)} + Pb^{2+} \qquad \text{(eq. 4.10)}$$

Even if the reaction displayed in eq. 4.10 occurs, an excess of calcium would have to be added in order to displace the equilibrium towards the formation of calcium sulfate, as the K_{sp} of lead (II) sulfate (1.7×10^{-8}) is three orders of magnitude smaller than the K_{sp} of calcium sulfate (2.4×10^{-5}). Considering this, the possibility that colloidal sub-micron particles are removed from solution by occlusion within the dirty gypsum sludge is very likely to occur.

4.1.7 Treatment of an emulated mining waste

Weak acid was chosen due to the high concentration of copper present. Other mining related effluents such as AMD do not contain copper above 100 mg L^{-1}. An emulated version of the waste was prepared using the major dissolved constituents of this waste as described in Section 2.4.

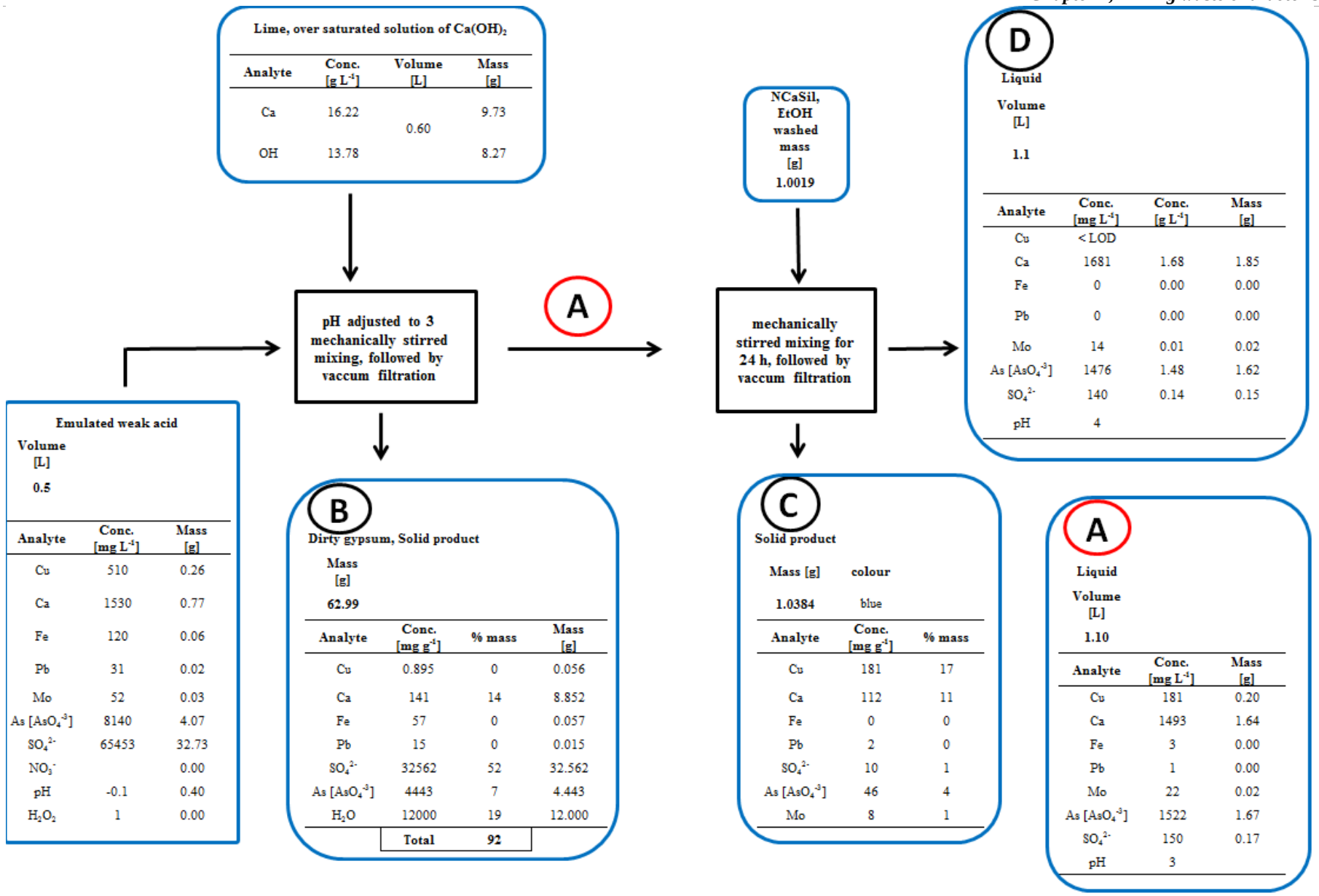

Figure 4.7: Emulated mining waste treatment flow sheet.

The emulated weak acid was treated to raise the pH to a value of 3. This step is important since all hydroxide groups on NCaSil are neutralized under this pH, thus not forming copper hydroxide on the surface. Additionally raising the pH above 3 may cause the precipitation of copper as a hydroxide salt.

This steps proves the possibility of attaching a NCaSil production plant and adsorption batch reactors to the previously mentioned BAMAG process. First it would include the precipitation of clean gypsum at pH 1 with a subsequent stage of raising the pH to 3 to produce the copper rich calcium silicate product. Hence two products, with commercial potential, would be produced on one hand clean gypsum and on the other a copper-rich calcium silicate. A scheme of such process is presented in appendix A-19

The addition of lime was expected to form insoluble compounds such as calcium hydrogen sulfate $Ca(HSO_4)_2$ and calcium hydrogen arsenate $Ca(HAsO_4)$ considering the K_{sp} and pK_a value for each of these salts. Nevertheless, other variation of the above salts could be formed such as calcium sulfate and calcium arsenate. The sample is called dirty gypsum mainly due to its content of arsenic making it useless for industrial application. In this case it was 52% wt of sulfate, 19% wt water, 14% wt of calcium and 7% arsenic as arsenate. In fact, 99.8% of the sulfate was removed from solution in this stage. Nonetheless, only 81% of the initial amount of arsenate was removed. Additionally, 50% of the initial mass of iron and lead was removed from solution. In the case of copper only 20% of the initial mass was removed from solution.

Figure 4.8 shows a SEM image at 2000x magnification of a solid sample of the filter cake recovered in stage B of Figure 4.7.

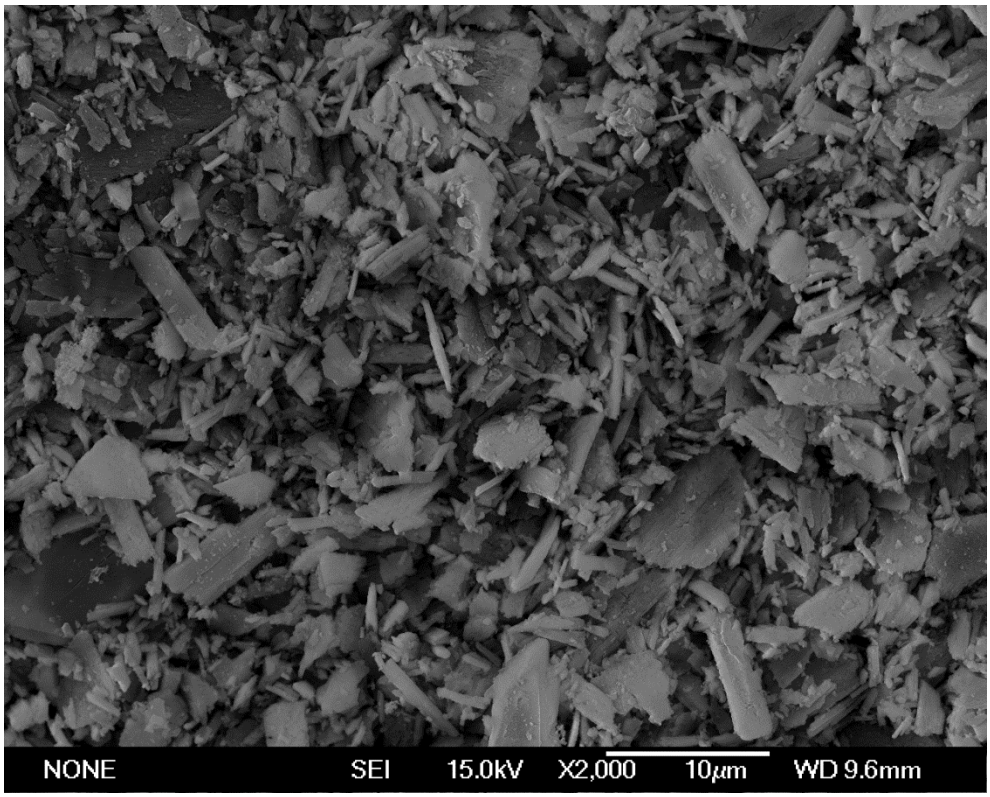

Figure 4.8: SEM image of the dirty gypsum produced at stage B in Figure 4.7.

The sample was covered by the flake-type morphology shown in the scanned region in Figure 4.8. Probably these crystals correspond to distorted prisms ranging in the size of a fraction of micrometre to 10 micrometre in length.

A backscatter image of the same region in Figure 4.9 shows that the atomic mass of the constituents is even throughout the surface of the sample. Nevertheless, there are some slightly brighter spots which are enclosed in white boxes in the picture.

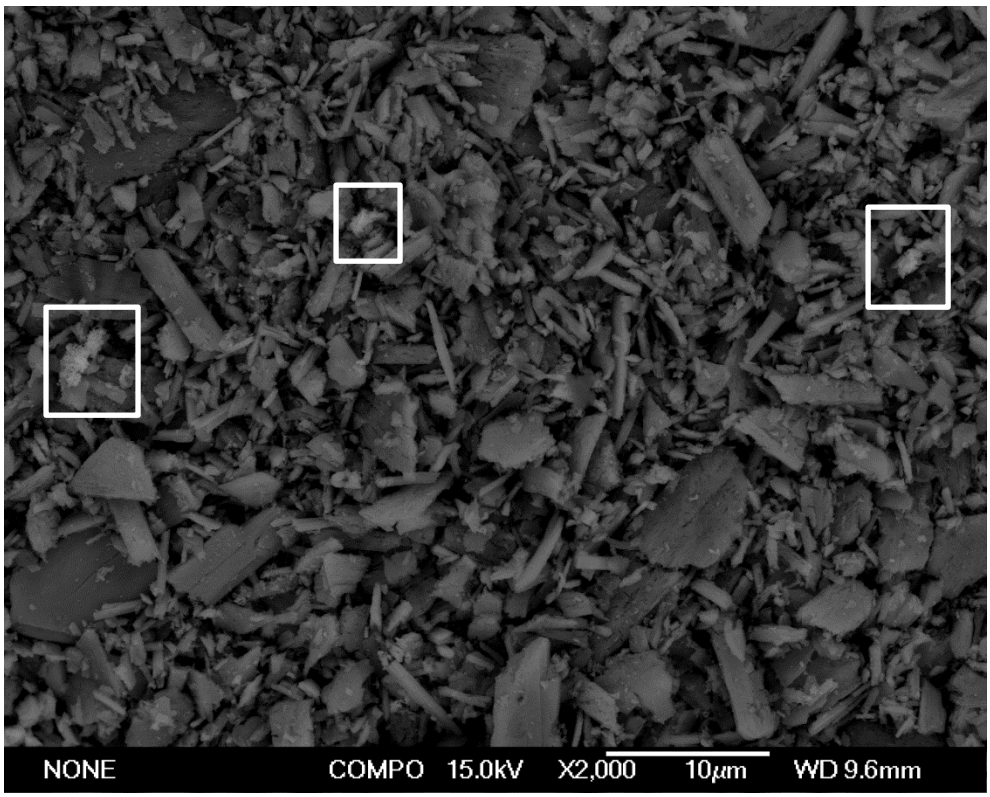

Figure 4.9: Backscattered electron image of the dirty gypsum produced at stage B in Figure 4.7.

As it was stated before it is logical to expect that the addition of calcium hydroxide will produce a combination of insoluble calcium sulfate and calcium arsenate salts. An EDS mapping was done to the same region shown in Figure 4.8 and Figure 4.9. Results are shown in Figure 4.10.

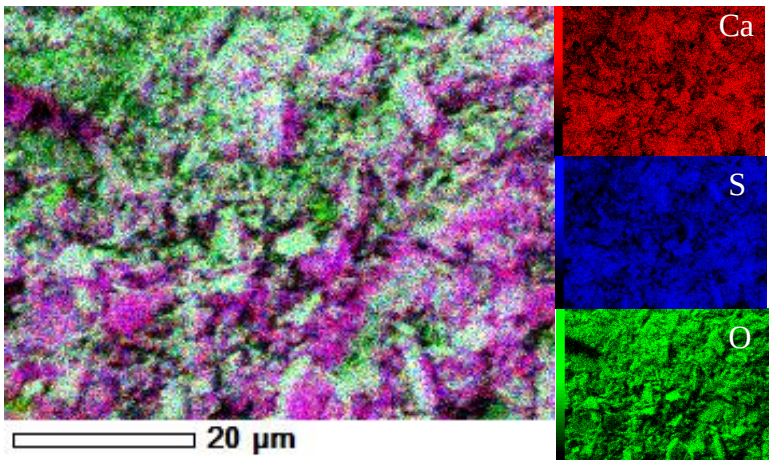

Figure 4.10: EDS map of Figure 4.9 with Cu (red), S (blue) and O (green).

The overlay picture of the three colours shows pink zones which indicate the presence of Ca and S. White colouration on the other hand shows the presence of Ca, S and O which is related to calcium sulfate or calcium hydrogen sulfate. As the lightest element the amount of oxygen might have been underestimated due to shielding effects by

calcium and sulfur. Green zones show no relation between oxygen and the other mapped elements. These may be related to other oxygen containing species such as arsenate or hydrogen arsenate.

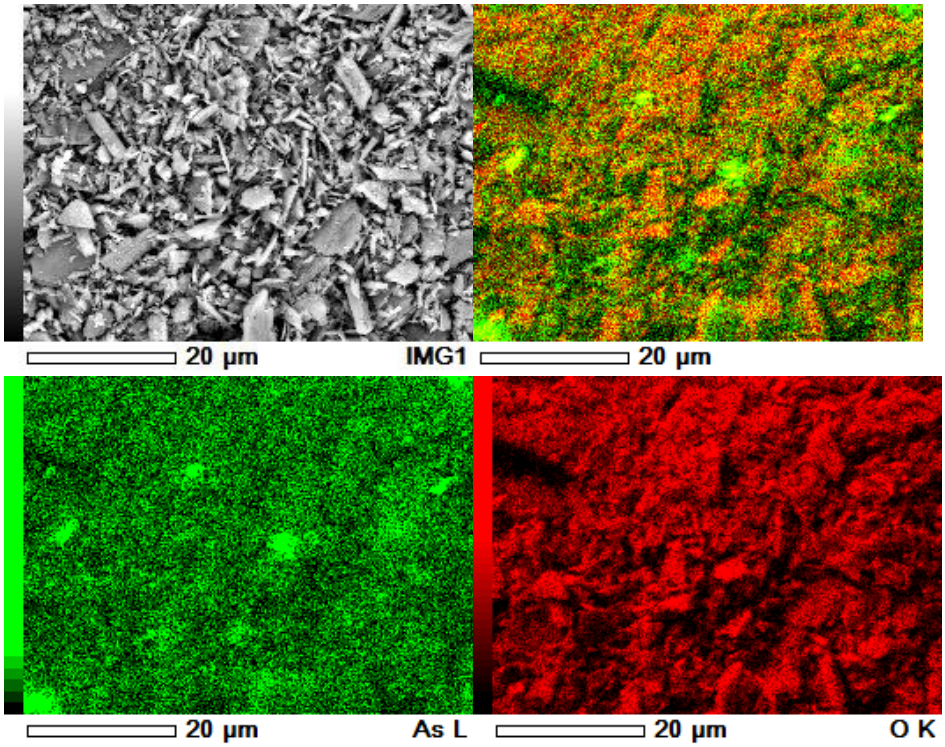

Figure 4.11: EDS map of Figure 4.9 for As (green) and O (red).

The same region was mapped for arsenic and oxygen to see there relation on the surface. The overlay image in Figure 4.11 shows that there is a correlation between the occurrences of these two elements on the surface of the sample being, up to a certain extent, evenly distributed throughout the sample surface. Nonetheless, there are few but intense green spots indicating arsenic rich species being present.

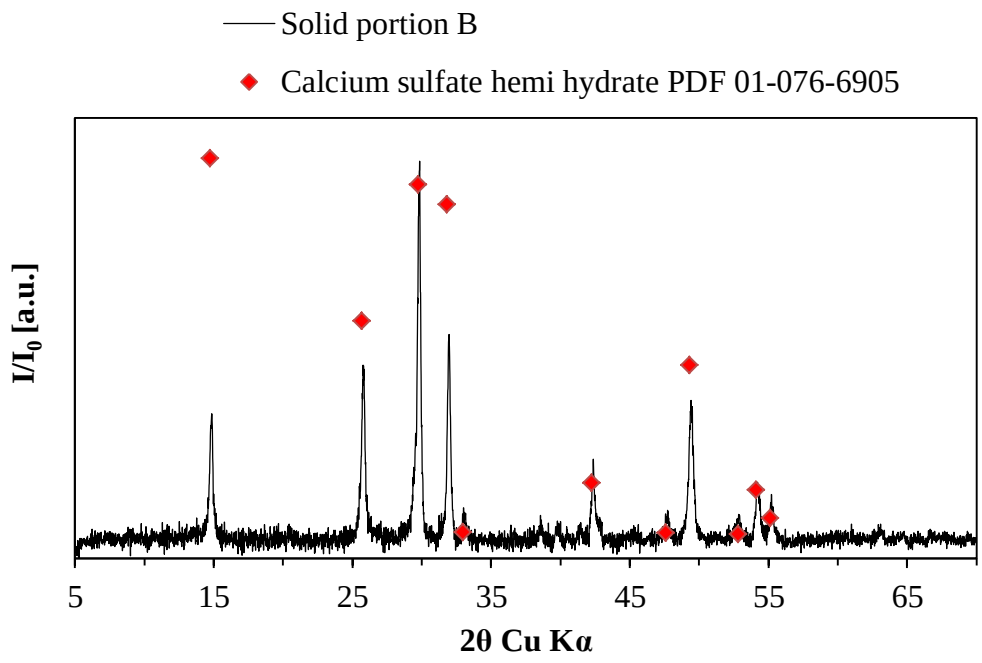

Figure 4.12: XRD pattern corresponding to solid fraction B in Figure 4.7.

Further information was gathered by grinding the sample and analysing it using XRD. The peaks scored 74 for $Ca(SO_4)_2 \cdot 1/2H_2O$ (PDF number 01-076-6905). The hemihydrate form may be due to the dehydration of calcium sulfate dihydrate during the preparation of the sample. This finding is consistent to the EDS mapping for this sample, although no diffraction peak associated to arsenic containing crystal could be found.

Following the diagram shown in Figure 4.7, after filtering the solid portion B, NCaSil was added to liquid A. This solution contained a concentration of copper of 181 mg L^{-1} since it was diluted by the addition of lime. Half of the initial amount of Pb and Fe remained in solution. 18.7% of the initial amount of arsenate was still in solution A. The addition of NCaSil resulted in the formation of a solid phase and a new liquid phase. A kinetic study of the uptake of copper, lead and iron using solution A was carried out and the results are presented in Figure 4.13. The three metals were effectively removed from solution (>99%). The reaction between NCaSil and copper ions was extremely fast, taking only 3 minutes to reduce the concentration of copper from 181 to 1.36 mg L^{-1}.

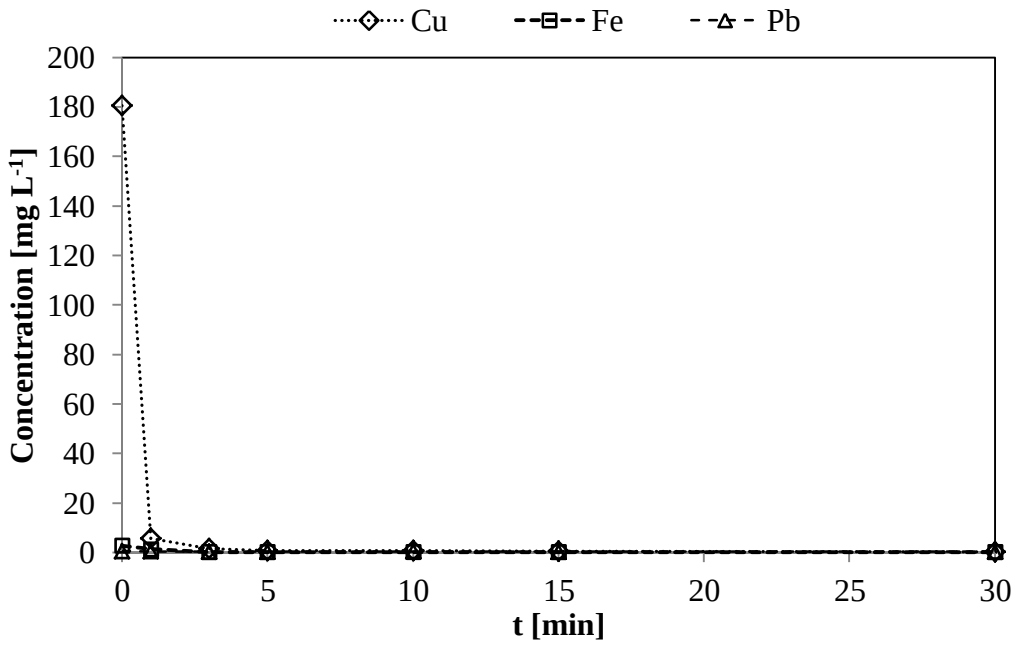

Figure 4.13: Kinetics of copper uptake by NCaSil from solution A in Figure 4.7.

The concentration of copper, lead and iron in solution D was below the detection limit. The pH of the solution was raised from 3 to 4 by the addition of NCaSil. In the case of arsenate and molybdenum, 97% and 64% of the initial amount in solution remained in solution, respectively. The amount of calcium in solution D is 13% higher than solution A due to Ca^{2+} leaching from NCaSil. The resulting solid C is rich in copper with low content of arsenate and sulfate as can be seen in Figure 4.7. This is an excellent result since even under extremely high concentrations of arsenate in solution and an adsorbent rich in calcium ions, only a small amount of arsenate precipitates. This would help in the real life operation to produce a copper rich solid with minor amount of impurities. NCaSil also exhibits a slight affinity towards removing molybdenum from solution, removing 36% of the amount present in solution A. The XRD pattern for solid portion C is shown in Figure 4.14.

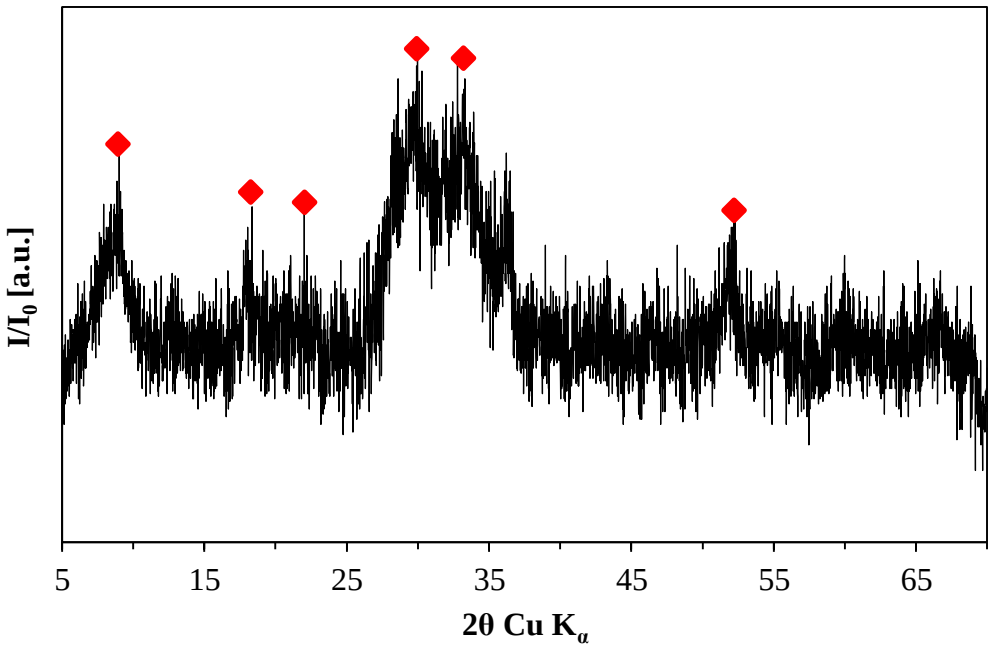

Figure 4.14: XRD pattern corresponding to letter C in Figure 4.7.

Although peaks did not match to any of the crystal structures in the database, peaks at 9.0°, 18.3°, 22.0°, 29.9°, 32.8° and 51.9° 2θ Cu K_α could be associated to poorly crystalline gypsum, NCaSil or posnjakite ($Cu_4(OH)_6SO_4$). Calcium carbonate can be discarded due to a pH value of 4 in solution D. Copper might be forming posnjakite as it was shown in Figure 3.32 at initial concentrations of copper near 2 mmol L^{-1} this mineral may develop. Although the final pH differs between these two samples, the results shown in Table 3.5 has a final pH value in the solution near 8 and the emulated mining waste had a value of 4. Therefore, the amount of OH^- groups available to form the crystal is larger in the former.

4.2 Chapter Conclusions

Weak acid is generated in two different plants during the cleaning and cooling of furnace gases using water scrubbers at the sulfuric acid plant of the El Teniente mine in Chile. The weak acid is composed of a liquid (supernatant) and solid phase (suspended solids). The supernatant contains a high concentration of total arsenic of 6.0 ± 0.8 g L^{-1} for Plant 1 and 6.5 ± 1.3 g L^{-1} for Plant 2. Sulfate concentrations over the studied period of time were 43 ± 10 g L^{-1} for Plant 1 and 69 ± 12 g L^{-1} for Plant 2. The higher concentration of arsenic and lower concentration of sulfate compared to those found in other smelters could be related to the lower metal sulfide and higher arsenic content in the ore being processed at El Teniente. Suspended solid concentrations showed large spikes on a few dates, which contributed to a large value for the standard deviation for the solids concentrations. Solid concentrations of 0.23 ± 0.63% wt for Plant 1 and 0.97 ± 0.95% wt for Plant 2 were reported for the period from April to October 2010. Overall, both plants operated almost all of the time within the control limits and exhibited very few concentration spikes over the studied period of time.

Chemical analysis of the supernatant showed that it had a low pH-value of 0.45 and contained a high concentration of heavy metals. Copper had the highest concentration with a value 562 mg L^{-1}. Taking in consideration the concentration of the different analytes the weak acid can be classified as an extremely acidic and high metal content waste.

Even though As and sulfate concentrations differ from those reported for other furnaces around the world, the measured parameters, such as arsenic, copper and sulfate, are still of the same order of magnitude as those described in the literature, for example those reported for the Toyo smelter in Japan.

High concentrations of copper in solution represent an estimated loss of 100 tons of this metal per year. A process such as the one utilized in Toyo's smelter in Japan, where copper ions are precipitated by the addition of NaHS should be considered.

SEM, EDS, powder-XRD and ICP-OES analysis of the suspended solids found in weak acid waste showed that this phase was mainly composed of sub-micron particles of anglesite ($PbSO_4$). This portion of the studied waste should be carefully investigated in future research to assess potential threats posed by these sub-micron particles and to suggest measures for preventing their release into the environment.

The treatment of the emulated weak acid with NCaSil is feasible at pH values of the weak acid above 3 and below 5. This prevents the rapid loss of structure of NCaSil which in consequence allows the adsorption of copper ions onto the surface. Additionally it also prevents removal copper ions during the pH adjustment stage as $Cu(OH)_2$ which is readily formed at pH above 5 in solution.

The uptake of Cu^{2+} onto NCaSil was extremely fast reaching equilibrium in only 5 minutes. The resulting solid had a low amount of arsenate and sulfate content demonstrating that the adsorption of copper ions is preferential making it suitable for industrial applications.

This process could be coupled to the one proposed by BAMAG GmbH which will actually optimize the utilization of this waste to produce two marketable products such as clean gypsum and a copper-rich calcium silicate. The remnant solution D may continue to the normal treatment of this waste that consists of precipitating arsenic containing species and disposal in a landfill.

83. H. Freundlich, *Grundzüge derkollodlehere*, **1925**, London, Methuen.

84. A. W. Adamson, *Physical Chemistry of Surfaces*. 2nd ed, **1967**, John Wiley & Inc.

85. M. A. M. Lawrence, N. A. Davies, P. A. Edwards, M. G. Taylor, and K. Simkiss, *Can adsorption isotherms predict sediment bioavailability?* Chemosphere, **2000**. 41(7): p. 1091-1100.

86. P. W. Atkins, *Physical Chemistry*, **1990**, Oxford University Press.

87. M. A. Sanchez. *Proceedings of the IV International Conference on Clean Technologies for the Mining Industry*. in *Environment & innovation in mining and mineral technology*. **1998**. Santiago, Chile: University of Concepción.

88. P. Ravenscroft, H. Brammer, and K. Richards, *Arsenic Pollution: A Global Synthesis*, **2011**, John Wiley & Sons.

89. L. M. Toovey, *The Top 10 Copper Producing Countries*. **2009**, Available from: http://copperinvestingnews.com/4147/the-top-10-copper-producing-countries/.

90. J. Newbold, *Chile's environmental momentum: ISO 14001 and the large-scale mining industry - Case studies from the state and private sector.* Journal of Cleaner Production, **2006**. 14(3-4): p. 248-261.

91. A. Black, D. Craw, J. H. Youngson, and J. Karubaba, *Natural recovery rates of a river system impacted by mine tailing discharge: Shag River, East Otago, New Zealand.* Journal of Geochemical Exploration, **2004**. 84(1): p. 21-34.

92. N. J. Wilson, Craw, D., Hunter, K., *Contributions of discharges from a historic antimony mine to metalloid content of river waters, Marlborough, New Zealand.* Journal of Geochemical Exploration, **2004**. 84(3): p. 127-139.

93. P. A. Weber, W. Skinner, J. B. Hughes, P. Lindsay, and T. A. Moore, *Source of Ni in coal mine acid rock drainage, West Coast, New Zealand.* International Journal of Coal Geology, **2006**. 67(4): p. 214-220.

94. L. Haffert, *Processes of attenuation of dissolved arsenic downstream from historic gold mine sites, New Zealand.* Science of the Total Environment, **2008**. 405(1-3): p. 286-300.

95. M. Ramirez, S. Massolo, R. Frache, and J. A. Correa, *Metal speciation and environmental impact on sandy beaches due to El Salvador copper mine, Chile.* Marine Pollution Bulletin, **2005**. 50(1): p. 62-72.

96. R. G. Trucco, *Heavy-Metal Concentration in Sediments from Tongoy and Herradura Bays, Coquimbo, Chile.* Marine Pollution Bulletin, **1990**. 21(5): p. 229-232.

97. Environmental Protection Agency U.S. *Technical Document, Acid Mine Drainage Prediction*, **1994**, Available from: http://www.epa.gov/epawaste/nonhaz/industrial/special/mining/techdocs/amd.pdf.

98. F. Valenzuela, J. Cabrera, C. Basualto, and J. Sapag-Hagar, *Kinetics of copper removal from acidic mine drainage by a liquid emulsion membrane.* Minerals Engineering, **2005**. 18(13-14): p. 1224-1232.

99. B. Aubé. *The Science of Treating Acid Mine Drainage and Smelter Effluents*. Available from: http://www.enviraube.com/tech/treatment_science.pdf.

100. M. E. Schlesinger, M. E. Davenport, M. J. King, K. C. Sole, and W. G. Davenport, *Extractive Metallurgy of Copper*, **2011**, Elsevier Science.

101. A. Ante, *Production of Marketable Gypsum from Weak Waste Acids - Saving Disposal Volume and Costs.* Erzmetall, **2005**. 2(58): p. 75-82.

102. A. Ante and S. Schonbrunner, *Possible use of weak acid gypsum from the BAMAG process.* Zkg International, **2007**. 60(8): p. 59-68.

103. J. L. Huisman, *Biologically produced sulphide for purification of process streams, effluent treatment and recovery of metals in the metal and mining industry.* Hydrometallurgy, **2006**. 83(1-4): p. 106-113.

104. C. M. Romo-Kröger, J. R. Morales, M. I. Dinator, F. Llona, and L. C. Eaton, *Heavy-Metals in the Atmosphere Coming from a Copper Smelter in Chile.* Atmospheric Environment, **1994**. 28(4): p. 705-711.

105. C. M. Romo-Kröger and F. Llona, *A Case of Atmospheric Contamination at the Slopes of the Los-Andes Mountain-Range.* Atmospheric Environment Part a-General Topics, **1993**. 27(3): p. 401-404.

106. G. Lagos, J. M. Lehuede, and M. Andia, *Sulfur dioxide abatement costs and compliance with health-based standards: the case of copper smelters.* Resources Policy, **2001**. 27(3): p. 147-155.

107. A. Roca, A. Morales, M. Cruells, and R. Bergo, *Treatment of copper flash smelter flue dusts for copper and zinc extraction and arsenic stabilization.* Hydrometallurgy, **2010**. 105(1-2): p. 148-154.

108. C. Nunez, F. Espiell, and A. Roca, *Recovery of Copper, Silver and Zinc from Huelva (Spain) Copper Smelter Flue Dust by a Chloride Leach Process.* Hydrometallurgy, **1985**. 14(1): p. 93-103.

109. M. Czaplicka and L. Buzek, *Lead Speciation in the Dusts Emitted from Non-Ferrous Metallurgy Processes.* Water Air and Soil Pollution, **2011**. 218(1-4): p. 157-163.

110. W. G. Davenport, M. King, A.K. Biswas, and M. Schlesinger, *Extractive metallurgy of copper*, **2002**, Pergamon.

111. T. Inami, K. Baba, and Y. Ojima, *Clean and high productive operation at the Sumitomo Toyo smelter*, **1990**. Sixth International Flash Smelting Congress, Brazil.

112. B. Lottermoser, *Mine wastes : characterization, treatment and environmental impacts*. 3rd ed, **2010**, Springer.

113. V. Ettler, Z. Johan, A. Baronnet, F. Jankovskya, C. Giller, M. Mihaljevic, O. Sebek, L. Strnad, and A. Bezdicka, *Mineralogy of Air-Pollution-Control Residues from a Secondary Lead Smelter: Environmental Implications.* Environmental Science and Technology, **2005**. 39: p. 9309-9316.

114. D. O. Cooney, *Adsorption Design for Wastewater Treatment*, **1999**, Lewis Publishers.

115. R. H. Perry and J. H. Perry, *Chemical engineers' handbook*. 4th ed., **1963**, McGraw-Hill.

116. C. Fonseca-Paris, *Estudio de la extracción de Cu(II) y Zn(II) desde soluciones acuosas ácidas mediante el empleo de membranas líquidas emulsificada, microencapsulación de extractantes y silicatos de calcio nanoestructurados*, **2009**, Universidad de Chile.

117. Sepragen Corporation, *Radial Flow Column*, cited **2012**, Available from: http://www.sepragen.com/page/Products-Chromatography-Columns.aspx.

118. T. Sparks, *Solid-Liquid Filtration: A User's Guide to Minimizing Cost & Environmental Impact, Maximizing Quality & Productivity*, **2011**, Elsevier Science.

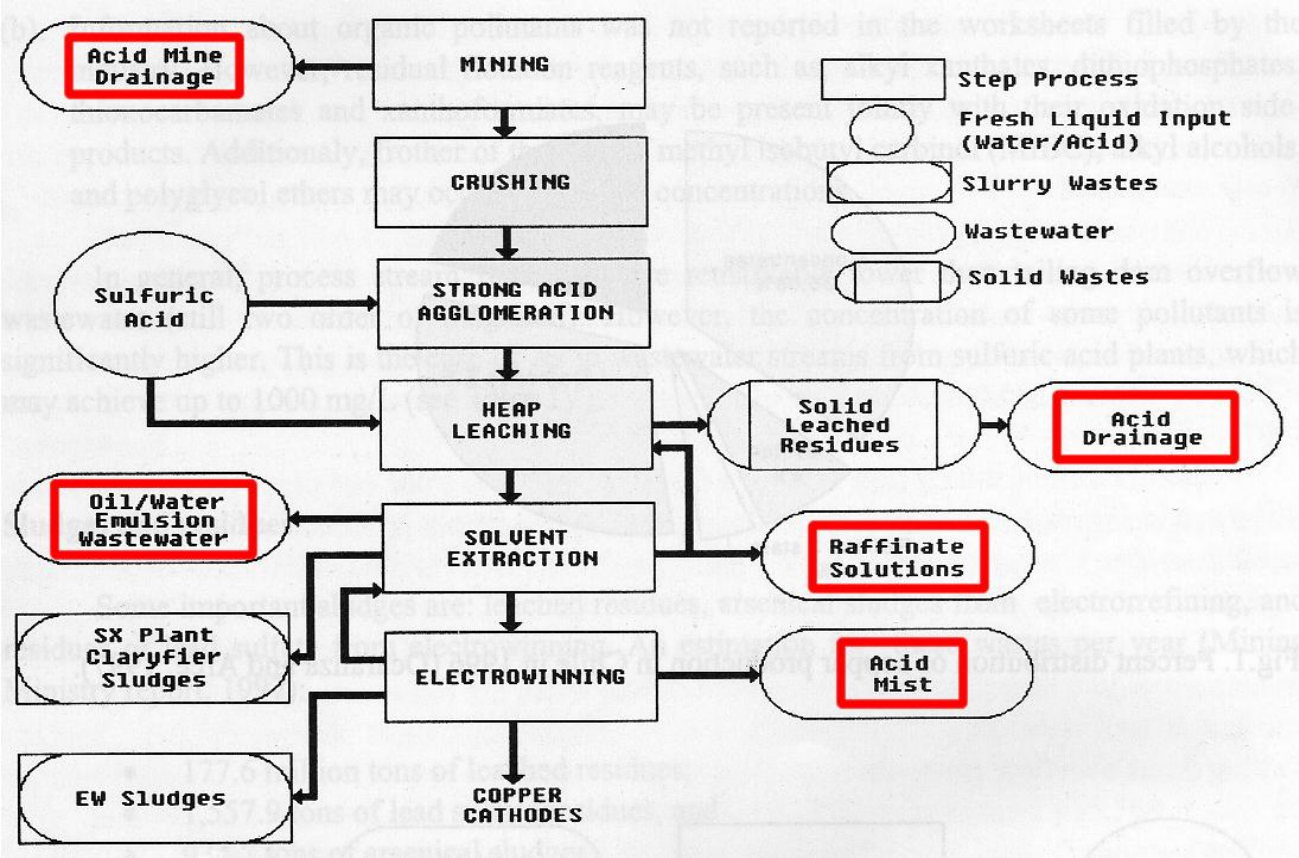

A-4: Diagram for oxidized and low grade copper sulfides processing in large scale mines in Chile [87]

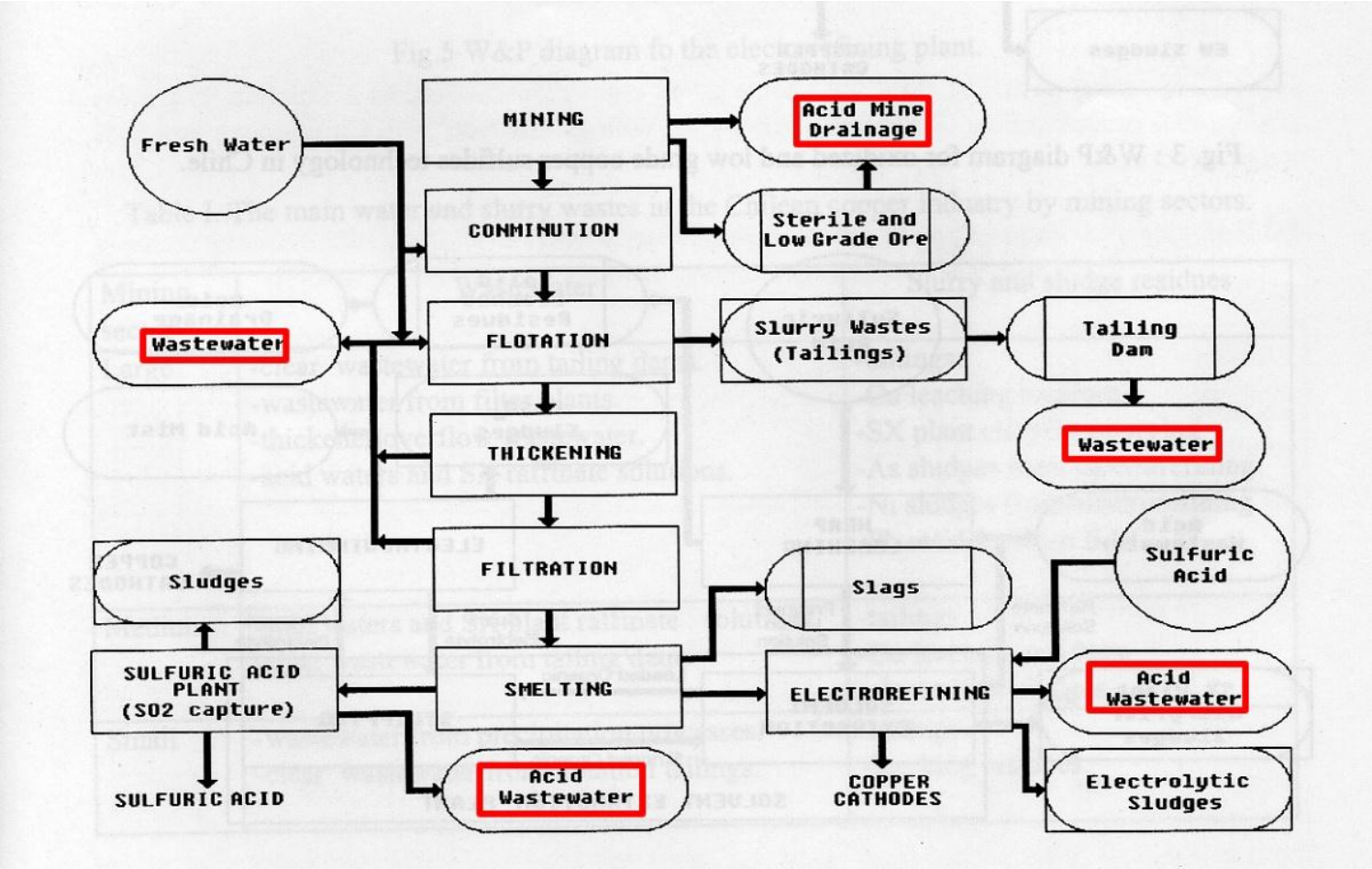

A-5: Diagram for high grade copper sulfides processing in large scale mining in Chile [87]

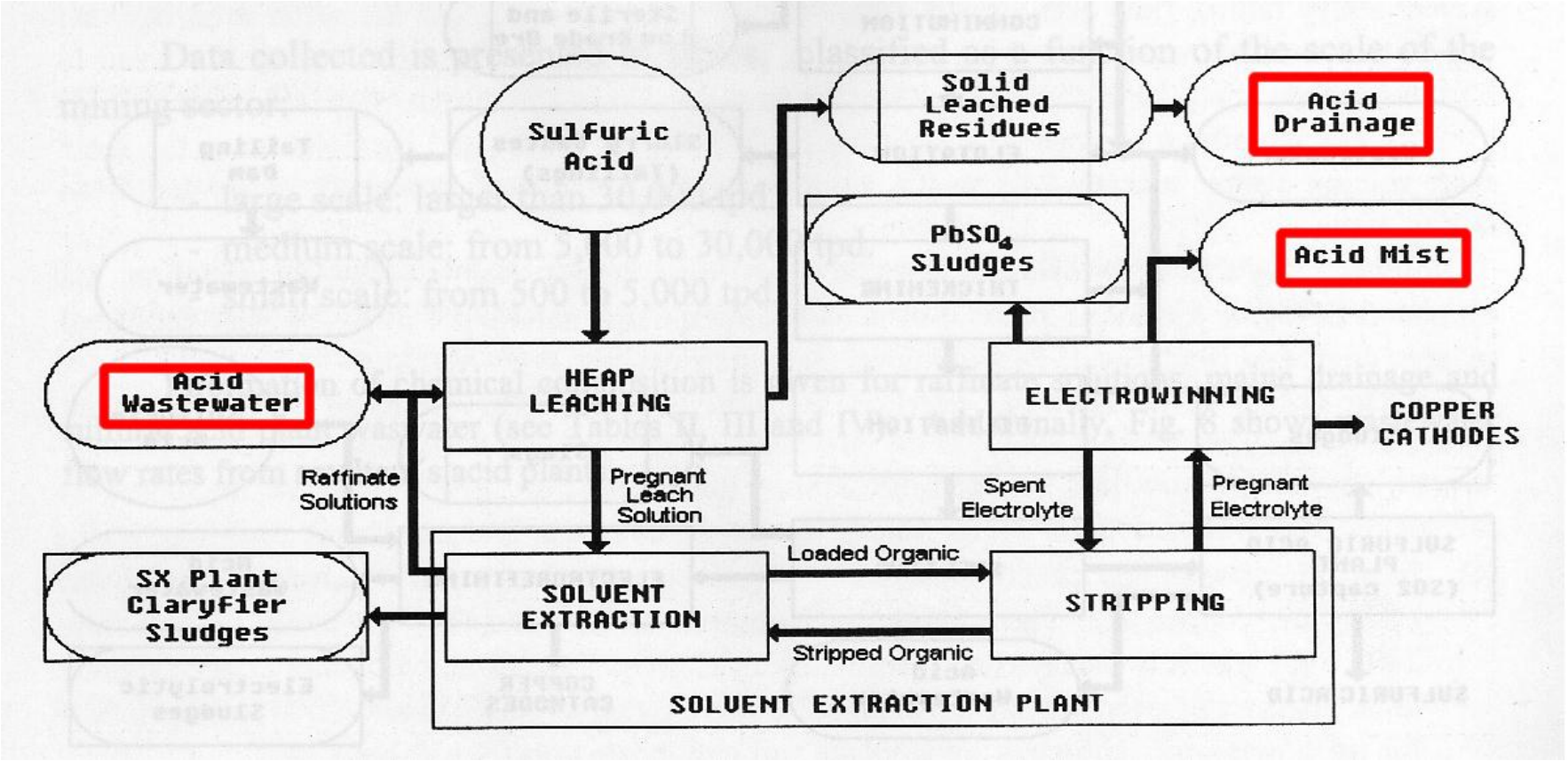

A-6: Diagram for Lixiviation – Solvent Extraction – Electrowinning plants for the purification of copper [87]

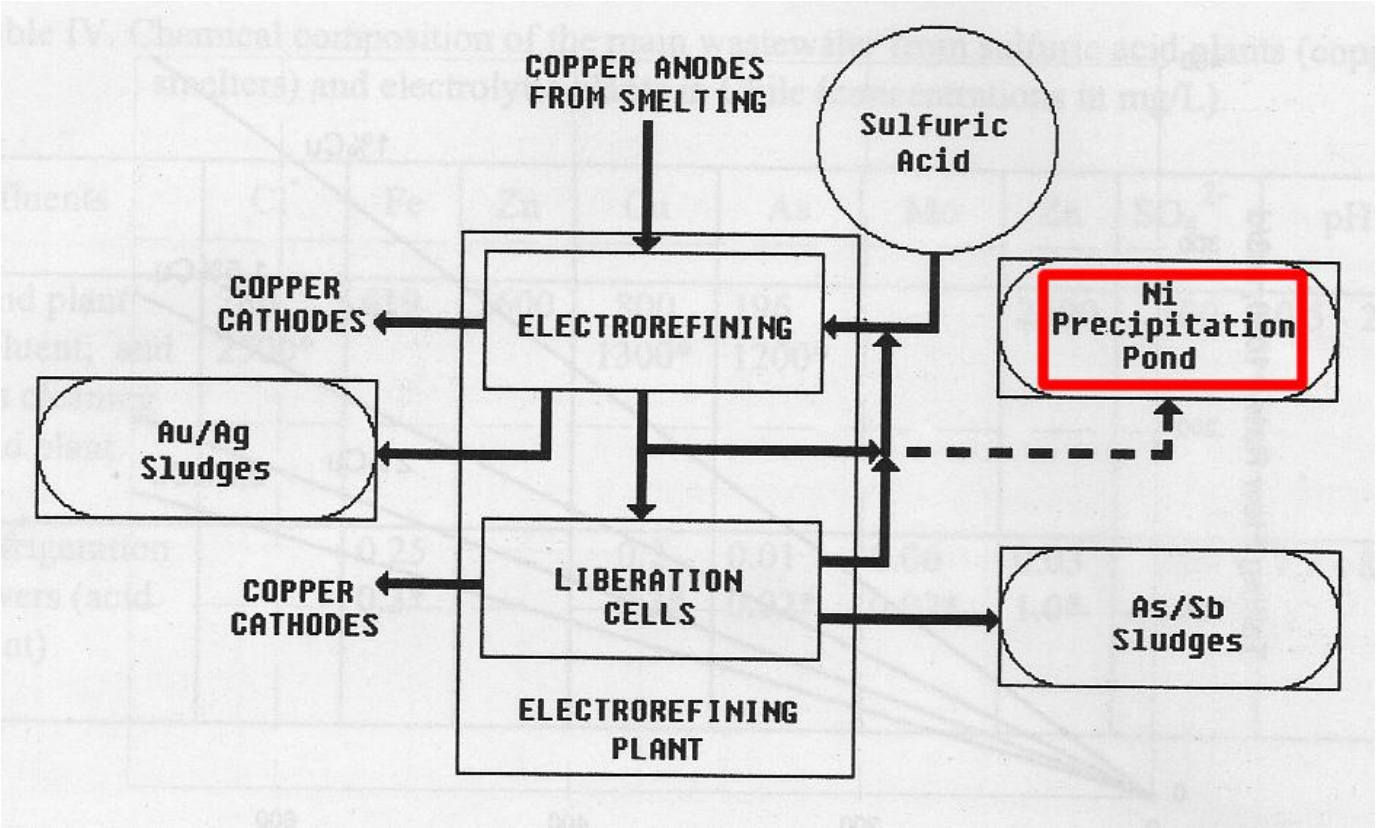

A-7: Diagram for a electrorefining plant for copper cathode production [87]

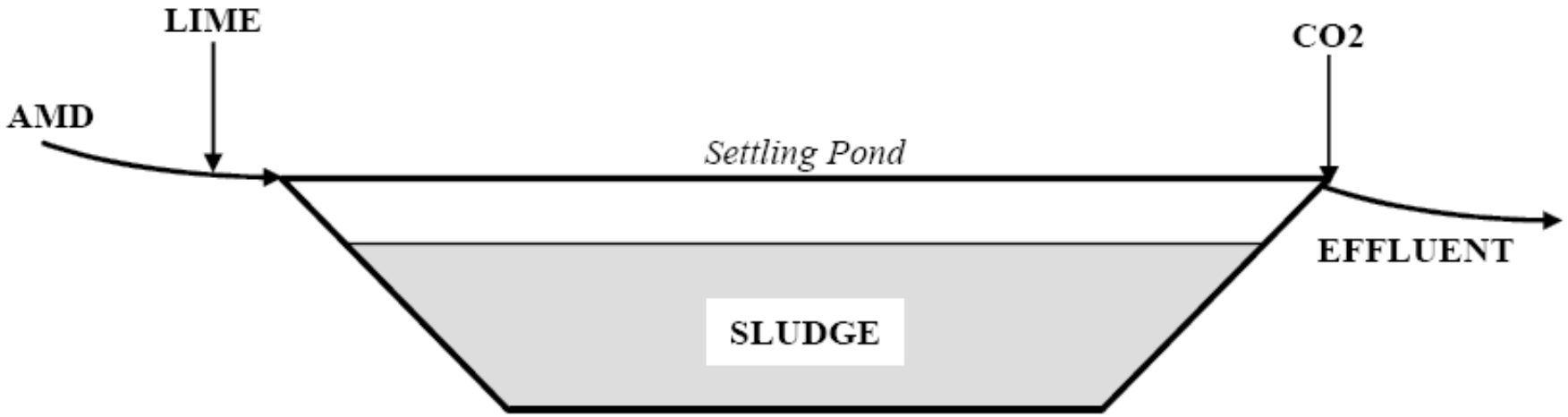

A-8: Settling pond for the treatment of mining tailings [99]

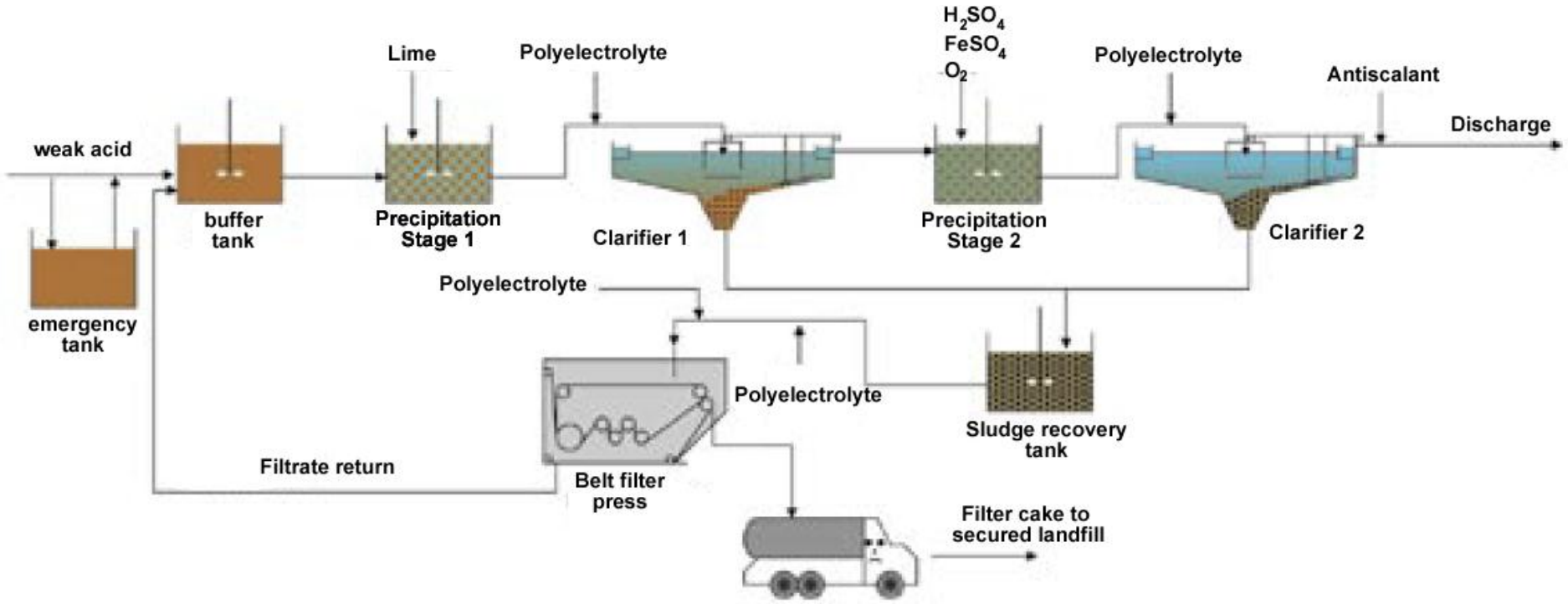

A-9: Copper smelter effluent (weak acid) treatment [101]

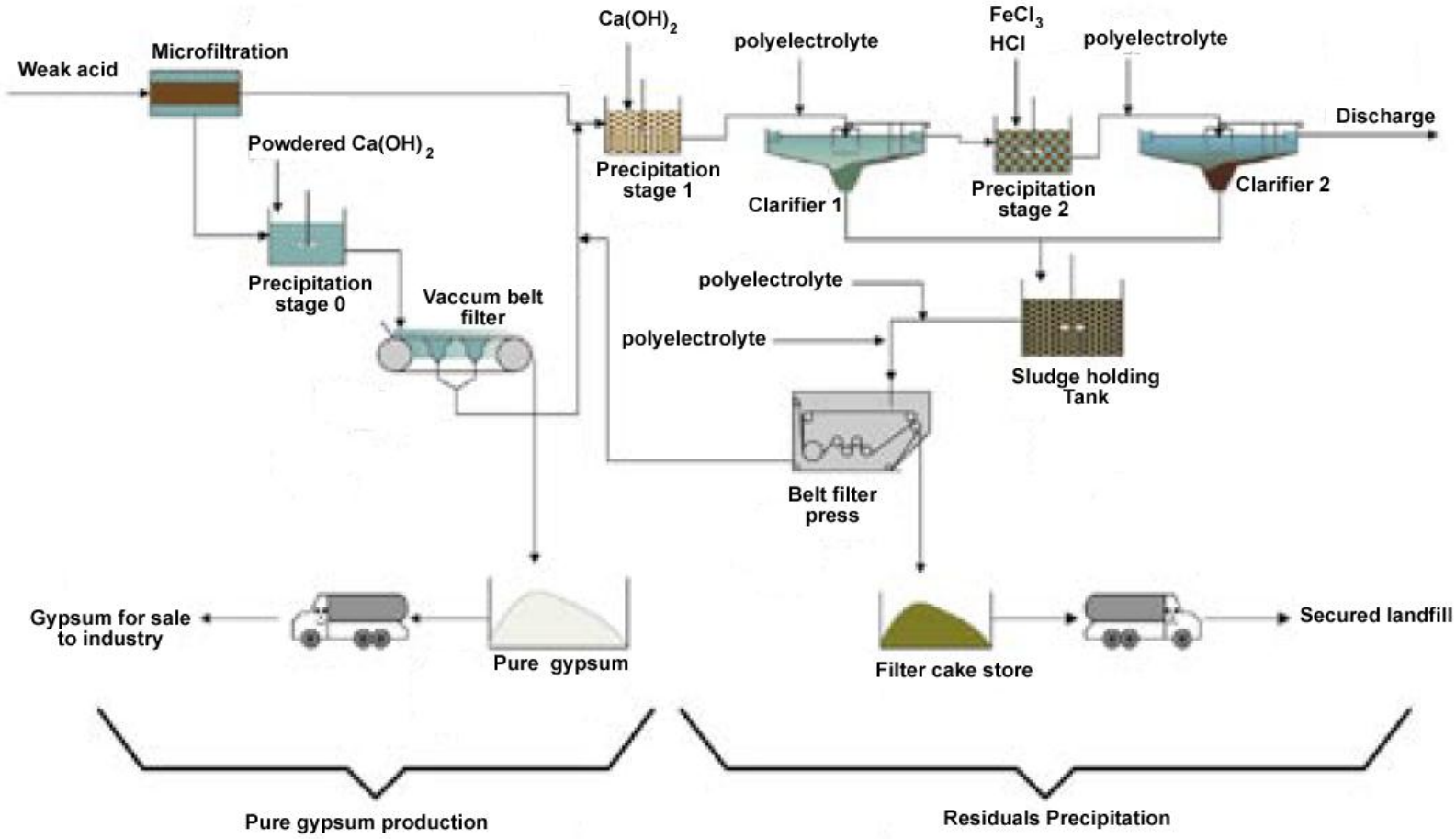

A-10: BAMAG GmbH process for treating weak acid mining waste [101]

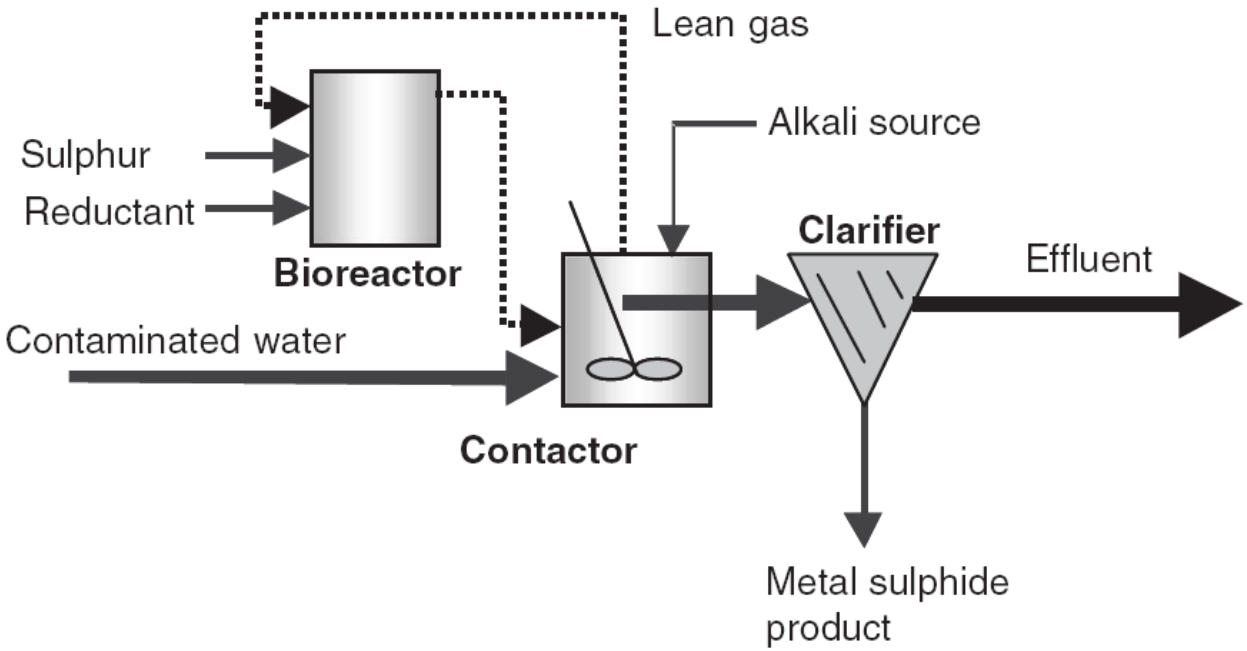

A-11: Biologically produce sulfur technology for mining waste water treatment [103]

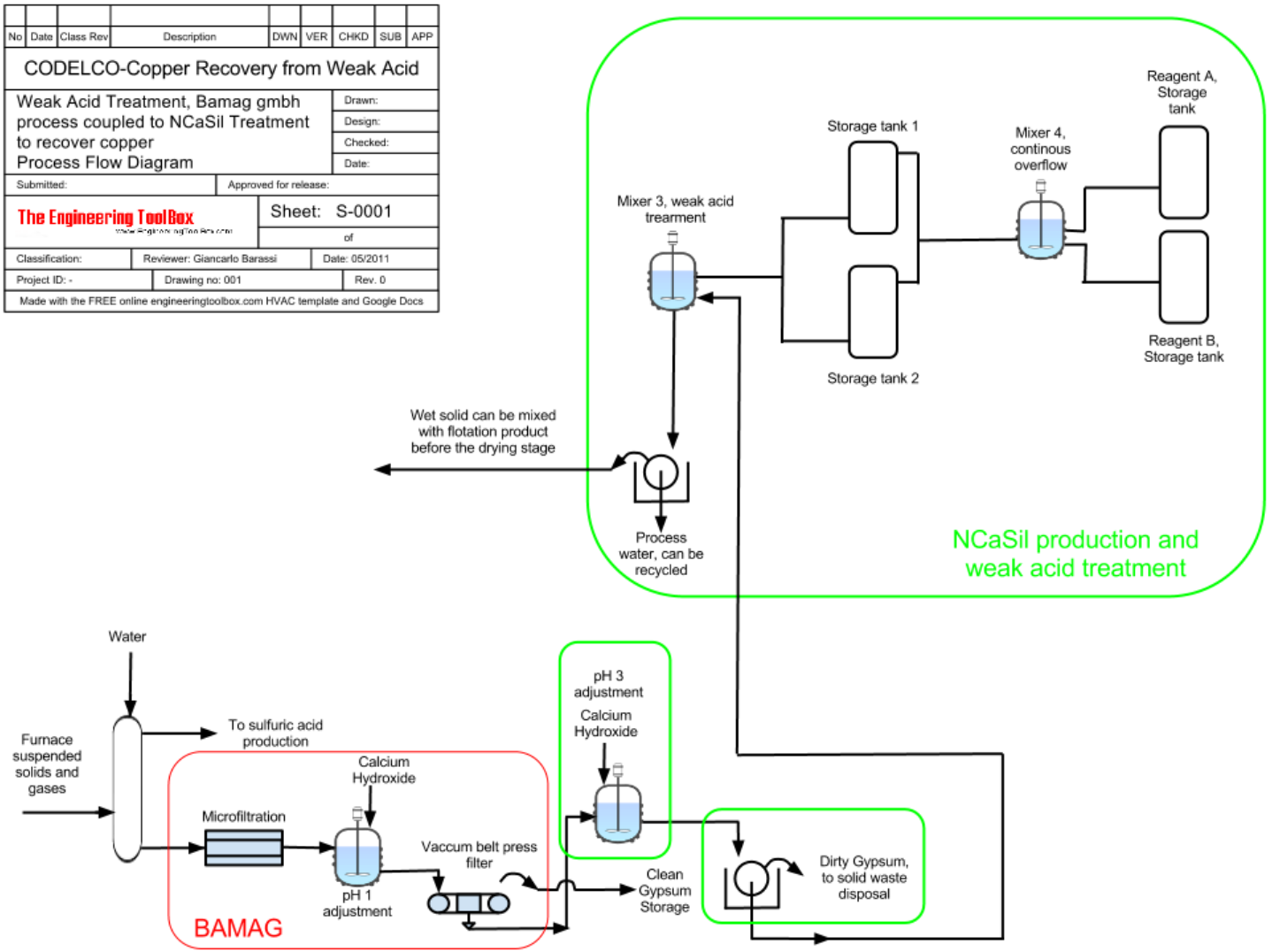

A-19: Coupled process for the production of clean gypsum and the recovery of Cu^{2+} using NCaSil.